Assessing land water storage dynamics over South America

Christopher E. Ndehedehe[a], Vagner G. Ferreira[b]

[a] *Australian Rivers Institute and Griffith School of Environment & Science, Griffith University, Nathan, Queensland 4111, Australia.*
[b] *School of Earth Sciences and Engineering, Hohai University, Nanjing, China*

Abstract

The underlying uncertainties in the prediction of freshwater evolutions in some regions can be induced by several unmitigated human actions, multi-scale climatic drivers, and dynamic physical processes. These factors have enduring hydro-ecological effects on the environments and combine to limit our understanding of large scale hydrological processes and impacts of climate on water availability. Considering the fact that several hydrogeological perturbations and disturbances have been reported during the last decade in South America (SA), a further assessment of continental land water storage is therefore warranted. In this study, a two-step regularization approach that combined the JADE (Joint Approximate Diagonalisation of Eigen matrices) algorithm and PLSR (partial least squares regression) was employed to assess GRACE (Gravity Recovery and Climate Experiment)-terrestrial water storage (TWS) over SA. Based on the Bartlett's statistics, significant independent patterns of SST (Sea Surface Temperature) anomalies from the Pacific and Atlantic oceans were used in the PLSR scheme to model the temporal evolutions of TWS ($2002-2017$) over twelve prominent river basins in SA. From the JADE rotation of TWS over SA, strong inter-annual changes in TWS observed over the Amazon basin and within its floodplain corridors were identified. The unabated mass loss in Patagonia ice-field caused by warming of the climate and other GRACE-hydrological signals were also retrieved from the JADE scheme. The rainfall-TWS relationship is considerably strong (r=0.80 at $0-2$ months lag) in much of tropical SA, including the Amazon basin and highlights the influence of climate variability in the region. Medium ($r = 0.40$) and moderately strong ($r = 0.60$) rainfall-TWS relationship were also found to be significant ($\alpha = 0.05$) but with up to 4 months lag and more in some basins. During the $2010-2017$ period, estimated TWS trends ($\alpha = 0.05$) showed a considerable fall in Orinoco (-38.48 ± 7.90 mm/yr) and Sao Francisco (-30.84 ± 4.17) while the strongest rise was found in Uruguay (28.28 ± 3.49 mm/yr). As the rainfall-TWS relationship is not statistically significant ($\alpha = 0.05$) in some areas, the spatial distribution of trends in TWS and rainfall, especially in some arid regions, which are

Email address: c.ndehedehe@griffith.edu.au (Christopher E. Ndehedehe)

inconsistent confirm possible impacts resulting from complex hydrogeological processes and/or anthropogenic influence. Further, in the modelling of TWS time series using the JADE-PLSR scheme, several validation skill metrics (e.g., R^2, Nash-Sutcliffe Efficiency) confirm the considerable agreements between predicted and observed TWS in the Amazon (R^2 = 0.95), Orinoco (R^2 = 0.94), Tocantins (R^2 = 0.91), and Chobut (R^2 = 0.88). However, GRACE-hydrological signals in some regions are somewhat complex given the relatively higher uncertainties in the multivariate models employed in this study.

Keywords: Rainfall, sea surface temperature, Amazon basin, partial least square regression, ENSO, Climate variability

1. Introduction

The knowledge of global freshwater response to critical stressors (e.g., human abstraction and climate) is an emerging aspect of freshwater science that is significant to model the influence of threats to water and food security (75, 92). However, the underlying uncertainties in the prediction of freshwater evolutions in some regions can be induced by non-climatic factors, e.g., earthquakes, land subsidence, and unmitigated human actions (e.g., 75, 24, 40, 17). Within the context of dynamic earth processes, South America, for instance, is a hub of frequent considerable crustal and lithospheric deformations, seismicity, and geo-hazards (see, e.g., 76, 27, 55, 54, 42, 91, 40, 51). These geodetic disturbances and the composite influence of climate and physical processes could have implications on surface mass variations and the acceleration of the water cycle.

In the light of the aforementioned perturbations on surface hydrology, time-variable geophysical signals observed by the Gravity Recovery and Climate Experiment (GRACE, 87) are expected to be driven not only by climate oscillations and key processes of inter-annual variability (e.g., 65, 64, 63, 22, 50, 70) but natural and other non-climatic elements, e.g., human water abstraction and deformations (e.g., 75, 15, 13, 24, 17). This assumption is anchored on the fact that apart from the redistribution in continental water storage, other dynamic processes such as gravitational tide in the solid Earth, post glacial rebound and variations in Antarctic and Greenland ice volumes cause significant changes in the Earth's gravity (e.g., 85, 94). Whereas a plethora of scientific reports on freshwater dynamics are mostly focused on climate variability related changes (e.g., 75, 6, 73, 88, 50, 70), very little attention is paid to improving our understanding of the possible contributions of non-climatic factors, especially those not related to groundwater abstraction.

For regions with frequent repeat cycles of such factors, freshwater dynamics is expected to be poorly understood. Hence, predicting freshwater systems at regional or continental scales require large scale assessment of TWS(terrestrial water storage) variations and an understanding of prominent drivers of surface hydrology. While this knowledge will lay the foundation for an efficient modelling framework for water resources, limited ground observations and the lack of a suitable modelling approach to characterize key hydrological metrics however, are some important constraints to such assessments. Further, the proliferation of dams and surface water developments for hydropower, agriculture and other relevant applications are gradually emerging as considerable drivers of TWS. In Africa, such impacts have been reported for the lake Volta and Victoria (see, 62, 56, 2). While the global expansion of dams and hydro-power stations are welcomed initiatives that could significantly boost global hydroelectricity capacity (101), they are also expected however, to have considerable impact on hydrological changes as is the case in Lake Volta (see, 62, 59), or over the Amazon basin where dam constructions are impacting on the ecosystems by modifying vital flood pulses[1].

Since the advent of GRACE, quantitative estimates of monthly changes in TWS (soil moisture, groundwater, surface water, wetlands, etc.) have been recovered across the globe. Because of its spatial resolution (90,000 km^2), the dynamics in multi-layered land water storage can be measured at global or regional scales with an accuracy of 15 mm expressed in terms of equivalent water height (26). Apparently, the preponderance of GRACE-hydrological studies in South America-SA (Figs. 1a and b) focused on some sections of the Amazon basin (see, e.g., 89, 50, 21, 34, 30, 31, 3, 46, 39). However, the validation of regional mass solutions of GRACE Level-1 data and the estimates of TWS over SA based on constrained least-squares method have been reported (35, 72). Considering the complex hydrogeological structures of SA (Fig. 1a), these studies emphasize the need to further assess the inter-annual variations of land water storage and the representation of dynamic processes in time-variable gravity observations. Given that SA accounts for nearly one fifth of global continental freshwater discharge (e.g., 50), a continent-wide assessment of GRACE-derived TWS has become necessary not only to improve our contemporary understanding of large scale hydrological processes, but to support the tracking and modelling of freshwater dynamics in the region.

Consequently, to improve our understanding of the spatial and temporal variations of extended GRACE-derived TWS (2002−2017) over SA, this study, localises GRACE-hydrological

[1] https://news.mongabay.com/2018/01/study-amazon-dams-are-disrupting-ecologically-vital-flood-pulses/

signals by rotating it towards statistical independence using the Joint Approximate Diagonalisation of Eigen matrices (JADE) algorithm (e.g., 60, 102, 12, 11, 18, 10). Given the lack of sufficient groundwater monitoring bores in many regions of the world, the JADE algorithm could be used to identify strong hydrological signals induced by droughts or even characterize groundwater variations from GRACE-TWS without using apriori information. For the first time, a partial least squares regression (PLSR) model is combined with JADE rotation and multi-linear regression to model GRACE-TWS over SA. The specific aims of this study are to (i) assess localised spatial and temporal variations of GRACE-derived TWS over SA through the rotation of prefiltered GRACE-hydrological signals, (ii) assess inter-annual variations in TWS in relation to precipitation, and (iii) predict temporal evolutions of GRACE-derived TWS over 12 prominent river basins in SA. To achieve this, localised sea surface temperature (SST) anomalies were used as input in a PLSR model. The assumption here is that strong ocean-land atmosphere interaction and the nearby oceans produce the systems that regulates precipitation. For most tropical systems, one key aspect of the hydrological cycle that shows an increasing acceleration is precipitation. Unprecedented anomalies in precipitation are expected to have considerable impacts on continental TWS variations. In general, this is the case given the widely reported influence and the feedback mechanism of anomalous warming of the surrounding oceans on inter-annual rainfall variations (e.g., 103, 64, 68, 66, 29). So, the PLSR model uncertainties in the simulation of TWS based on leading SST modes from the Pacific and Atlantic oceans are assessed in relation to observed continent-wide and basin-scale long terms trends in TWS and rainfall. More details on the methodological development and applications are highlighted in Section 3.

2. Data

2.1. Global Precipitation Climatology Centre precipitation

The Global Precipitation Climatology Centre (GPCC, 78) based precipitation data provides monthly grids of global land-surface precipitation. The 0.5° ∘ x 0.5° GPCC data used in this study to examine TWS-rainfall relationship was downloaded from the GPCC data portal (www.ftp.dwd.de/pub/data/gpcc/html/downloadgate.html) and covers the period between 2002 and 2017. The data is one of the most reliable observational reference precipitation product derived from gauge observations across the globe and has been widely used in several hydro-climatic studies (1, 5).

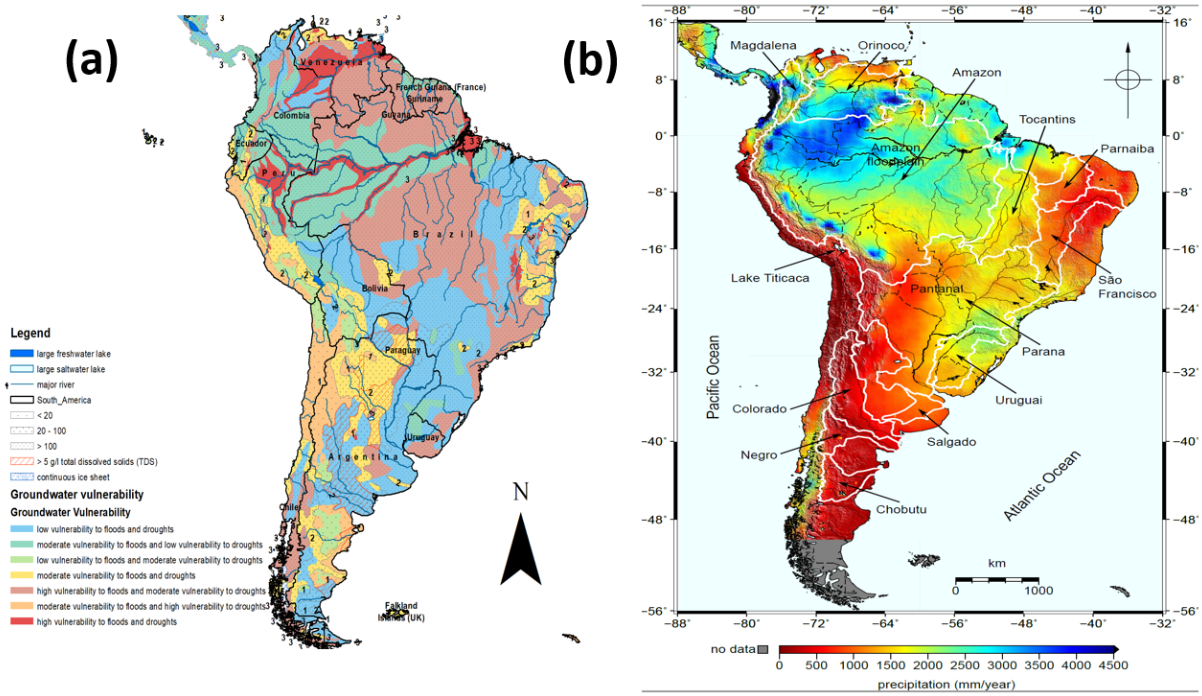

Figure 1: Map showing countries, rivers, and groundwater aquifers in South America. (a) The hydrogeological map of South America indicating aquifers, rivers, lakes and groundwater vulnerability areas. The Classification of groundwater recharge (mm/a) rates are in numbers (e.g., 2(= 20 - 100)). The aquifer maps and hydrological units (river distribution networks and lakes) are those of World-wide Hydrogeological Mapping and Assessment Programme produced under the Global Groundwater Vulnerability to Floods and Droughts project (WHYMAP GWV © BGR & UNESCO 2015). (b) The prominent river basins in South America and the network of transboundary rivers in each wetland and the annual distribution of rainfall from the Tropical Rainfall Measuring Mission satellite-based precipitation (2003 – 2016).

2.2. Land water storage assessment using GRACE mascons

Gravity Recovery and Climate Experiment-derived TWS is now one of the most vital tools in hydrological research, specifically in monitoring sub-surface water storage, aquifer system processes, and evaluating groundwater resources (see, e.g., 13, 62, 25, 86). The applications of GRACE data in hydrology research globally is growing and well documented (see, 41, 100, and the references therein) and is only summarised here. In this study, the GRACE mass concentration solutions (mascons), which solves for monthly gravity field variations in terms of 40,962 geodesic grid tiles over the Earth (77) were used for estimating land water storage over SA. The mascon blocks were down-sampled to a spatial resolution of 0.5° -by-0.5° in order to facilitate the regional averaging whereas the re-sampled cells (i.e., 0.5° -by-0.5°) is still limited to the nominal resolution of GRACE, which is about 300 km. The CSR mascon approach is based on two-step process (using an intermediate solution in a first step for deriving a time-variable regularization matrices for estimating the mascon solution in a last step), which allows the development of a time-variable regularization purely based on GRACE data. This regularization prevents the signal leakage into the oceans (77). The constrained regional water mass solutions used over South America showed they offer a reliable geographical location of hydrological structures (35). Apparently, these pre-processed GRACE products simplify the use of GRACE TWS observations for several hydrological and water resources applications. More details regarding the derivation of the mascon solutions and its performance metrics have been documented by Watkins et al. (95). The mascon data (2002 – 2017) was accessed from the CSR data portal `(http://www2.csr.utexas.edu/grace/RL05_mascons.html)` in its Release 05 (RL05). The use of GRACE mascons is gradually emerging in global freshwater analyses and offer the opportunity to implement geophysical constraints with ease, which in turn help to filter out noise from the level 2 GRACE data (e.g., 96). Apart from not requiring rigourous pre-processing protocols such as destriping and smoothing, it has been argued that the mascon solutions provide similar results consistent with other global GRACE products (e.g., 7). River basin estimates of TWS values $\overline{TWS}$ were recovered from the global mascon solutions by using the area weighted average approach, i.e., the approximated area of the basin (region) as (e.g., 62)

$$\overline{TWS}(t) = \frac{1}{A}\sum_{i=1}^{n}\overline{TWS}(\phi_i, \lambda_i, t)A_i, \tag{1}$$

where n is the number of cells within the basin, A_i is the area of each cell i, A is the total area of the basin and ϕ_i and λ_i are the corresponding latitudes and longitudes of the center of each grid cell, respectively.

2.3. Sea surface temperature anomalies

The Sea Surface Temperature (SST) data (monthly means from 2002 to 2017) used in this study is the NOAA's Optimum Interpolation SST V2 and was downloaded from NOAA's portal (`https://www.esrl.noaa.gov/psd/data/gridded/data.noaa.oisst.v2.html`). The influence of SST anomalies on land water storage in tropical regions have been reported (e.g., 50, 21, 64). So significant modes of localised SST variability from the Atlantic and Pacific oceans were used as predictors in the partial least square regression model (Section 3.3). Except in cases of human water management (e.g., water transfers), SST is a key predictor of rainfall and water availability because de Linage et al. (21) identified several studies that showed evidence of the interactions between SST and Intertropical Convergence Zone, which resulted in the severe droughts of 2005 and 2010 in the central and western Amazon.

3. Methods

3.1. Pre-orthogonalization of terrestrial water storage

The pre-orthogonalization (i.e., pre-filtering) of terrestrial water storage (TWS) was achieved using the principal component analysis (PCA, 58, 44). A scree plot analysis and the Bartlett's test statistics (53, 82) were employed to identify the statistically significant orthogonal modes of variability from the PCA scheme. Before the decomposition of TWS over SA, these test statistics ensured that only the significant orthogonal modes necessary to explain the non-random variations in TWS at 95% confidence level were used as inputs. The filtering of TWS using this method is given as (e.g., 58),

$$\mathbf{X}(t) = \sum_{k=1}^{n} a_{(k)} \mathbf{p}_k \tag{2}$$

where $a_{(k)}$(t) are the temporal variations also called expansion coefficients (or sometimes standardised scores) and $\mathbf{p}_k$ are the corresponding spatial maps (empirical orthogonal functions-EOF loadings). The leading orthogonal modes of TWS (a combination of the temporal and spatial patterns) retained for further rotation are the first few pairs obtained from this technique. Each expansion coefficients represents a fraction of the total variation that is proportional to the amount of covariance in time explained by each eigenvector (EOF).

3.2. Decomposition of TWS using the Joint Approximate Diagonalisation of Eigen matrices

The JADE (Joint Approximate Diagonalisation of Eigen matrices) technique is a generic algorithm for blind source separation (e.g., 12, 11, 18, 10). There are several formulations of the JADE algorithm based on three cost functions (e.g., 102) , however, on grounds of numerical and computational efficiency, the approach in this study was based on the joint diagonalization of the fourth order cumulant matrices as formulated and implemented by Cardoso (11) and Cardoso and Souloumiac (12). After the pre-orthogonalization of TWS using the PCA tool, which yielded significant orthogonal modes of TWS, the fourth order cumulant matrices were then estimated. These cumulants provide the suitable matrices to be diagonalized before a rotation towards statistical independence. In this study, the JADE algorithm fully detailed in previous studies (e.g., 102, 11, 12) was used to rotate the PCA-regularised data matrix $\mathbf{X}$ (i.e., Eqn. 2). Through a contrast optimization by the joint diagonalization approach, the rotated cumulant matrices resulted in well localised spatial maps $\mathbf{M}$, and temporal patterns $\mathbf{A}$, as: (e.g., 60)

$$\mathbf{X}_{TWS}(x, y, t) = \mathbf{AM}, \tag{3}$$

where (x, y) are pixel locations, t is the monthly time step. $\mathbf{A}$ is also known as independent components, which is unit-less since it has been normalised using its standard deviation while the corresponding spatial patterns $\mathbf{M}$, have been scaled using the normalised independent components (i.e., $\mathbf{A}$). Note that SST anomalies over the Pacific and Atlantic oceans were also subjected to the JADE process before use in the partial least squares regression (PLSR) model.

Although one could argue that working with basin-wise analysis of TWS in the continent is rather easy, the JADE technique is employed to support the localisation (both spatial and temporal) of GRACE hydrological signals that could be masked by other leading signals resulting from strong rainfall seasonality and surface flow from other hydrological regions (typical of the Amazon floodplain). So, the JADE analysis is essential to unpack hydrological elements (signals) in this region, which are largely characterized by rainfall, changes in floodplain rivers and complex hydrological processes. This method was efficient in the Volta basin where the Lake Volta shows strong gravitational signatures in the GRACE observations. The JADE rotation facilitated an understanding of the pseudo increase in TWS over the Volta basin caused by water impoundment of the Lake at the Akosombo dam despite more than a decade decline in observed rainfall (62). Through an innovative combination of this method with partial least squares regression (Section 3.3.1), this study attempts to provide further understanding related to both climate and non-climatic processes that provide constraints on freshwater availability in South America.

Furthermore, the linear rates (trends) in observed time series of estimated TWS over each river basin were estimated using the Sen's slope (80) estimator since it is robust and resistant to outliers. Sen slope (S_i) is the median overall values of the whole data and is estimated as

$$S_k = \text{Median}\left(\frac{P_j - P_i}{j - i}\right), \qquad \text{for} \qquad (1 \leq i < j \leq n), \tag{4}$$

where P_j and P_i represents data values at time j and i ($j > i$), respectively while n is the number of observations in the time series. To assess the significance of observed trends, the null hypothesis of no trend, H_0, was tested at $\alpha = 0.05$ using the Man-Kendall's test (52, 45). As one of our key objective here is to also assess TWS-rainfall relationship, the spatial distribution of trends in TWS with rainfall was examined to understand hydrological processes of the region.

3.3. Parameter estimation techniques

3.3.1. Partial least squares regression model

The partial least squares regression (PLSR) model is a double barrel multivariate tool as it combines features from PCA and MLRA (multi-linear regression analysis). As opposed to these multivariate techniques, PLSR is a better choice for analysing high-dimensional data because of its robustness and adaptability (e.g., 14, 20). PLSR looks for latent vectors, which performs a simultaneous decomposition of independent variable, $\mathbf{X}$ and response variable $\mathbf{Y}$ (e.g., 49, 99). These PLSR components are so determined to maximize the covariance between the two variables whilst complying with certain orthogonality and normalization constraints (20). In a simple formulation of the PLSR model (e.g., 14), the data elements $\mathbf{x}_i = [x_{i1}, x_{i2}, x_{i3}.., x_{ip}]' \in \Re^p$ $(i = 1, 2, 3, .., n)$ with n as the observation samples and $\mathbf{y}_i = [y_{i1}, y_{i2}, y_{i3}.., y_{iq}]' \in \Re^q$ $(i = 1, 2, 3, .., n)$ where n is the corresponding dependent samples. Then the independent variable, $\mathbf{X} = [\mathbf{x}_1, \mathbf{x}_2, \mathbf{x}_3.., \mathbf{x}_n]' \in \Re^{n\times p}$ and the response variable $\mathbf{Y} = [\mathbf{y}_1, \mathbf{y}_2, \mathbf{y}_3.., \mathbf{y}_n]' \in \Re^{n\times q}$. The centered (i.e., removing the mean) data matrices $\mathbf{X}$ and $\mathbf{Y}$ are decomposed as (e.g., 14, 99),

$$\mathbf{X}_{n\times p} = \mathbf{t}_{n\times 1}\mathbf{p}'_{p\times 1} + \mathbf{E}_{n\times p}, \quad \mathbf{Y}_{n\times q} = \mathbf{u}_{n\times 1}\mathbf{q}'_{q\times 1} + \mathbf{F}_{n\times q}, \tag{5}$$

where $\mathbf{t}$ and $\mathbf{u}$ are latent vectors for the n observations, $\mathbf{p}$ and $\mathbf{q}$ are the loading vectors while $\mathbf{E}$ and $\mathbf{F}$ are the residual matrices. PLSR model maximizes the squared covariance between the latent vectors ($\mathbf{t}$ and $\mathbf{u}$) and obtains the projection vectors $\mathbf{w}$ and $\mathbf{h}$ as $\mathbf{t}$=$\mathbf{Xw}$ and $\mathbf{u}$= $\mathbf{Yh}$. Lewis-Beck et al. (49) mentioned other ways of choosing the latent vectors and highlighted the iterative process of finding the latent vectors until $\mathbf{X}$ becomes a null matrix. If a linear association exist between $\mathbf{t}$ and $\mathbf{u}$ (e.g., 14, 99, 20), Eqn 5 above can be updated as

$$\mathbf{X} = \mathbf{tp}' + \mathbf{E}, \quad \mathbf{Y} = \mathbf{tq}' + \mathbf{F}. \tag{6}$$

And through a least square solution, $\mathbf{p}$=$\mathbf{X}'\mathbf{t}(\mathbf{t}'\mathbf{t})^{-1}$ and $\mathbf{q}$=$\mathbf{Y}'\mathbf{t}(\mathbf{t}'\mathbf{t})^{-1}$ can be solved. The regression between $\mathbf{X}$ and $\mathbf{Y}$ results in c projection vectors and a set of weights, $\mathbf{W} = [\mathbf{w}_1, \mathbf{w}_2, \mathbf{w}_3.., \mathbf{w}_c]$. The latent components or factor scores can be obtained as (14, 20), $\mathbf{T} = [\mathbf{t}_1, \mathbf{t}_2, \mathbf{t}_3.., \mathbf{t}_c]$ while the loading matrices are formulated as $\mathbf{P} = [\mathbf{p}_1, \mathbf{p}_2, \mathbf{p}_3.., \mathbf{p}_c]$ and $\mathbf{Q} = [\mathbf{q}_1, \mathbf{q}_2, \mathbf{q}_3.., \mathbf{q}_c]$. If Eqn 6 is rewritten as

$$\mathbf{X} = \mathbf{TP}' + \mathbf{E}, \quad \mathbf{Y} = \mathbf{TQ}' + \mathbf{F}, \tag{7}$$

then, from

$$\mathbf{T} = \mathbf{XW} + \mathbf{E}, \quad \mathbf{Y} = \mathbf{XWQ}' + \mathbf{F}, \tag{8}$$

the final standard PLSR relation between the predictor data matrix ($\mathbf{X}_{SST}$) and response ($\mathbf{Y}_{TWS}$) variables is

$$\mathbf{Y} = \mathbf{X}\beta + \mathbf{F}, \tag{9}$$

where $\beta = \mathbf{WQ'}$ is the PLSR coefficients. After this multivariate calibration, the modelling of TWS for each river basin (TWS_{RB}) over South America is subsequently obtained as

$$TWS_{RB} = \beta SST_{Localised\ modes} + Y_{res}. \tag{10}$$

The predicted TWS series were compared with the observed using several validation metrics and statistical index of model performance, i.e., Nash–Sutcliffe model efficiency (NSE), refined index of agreement (IA), coefficient of determination (R^2) and root mean square error (RMSE). Statistical details about the modified IA and the NSE coefficients are available for interested readers (e.g., 98, 57). Further, the Jargue-Bera statistical normality test (43) is an additional skill metric that was employed to validate the PLSR model output by evaluating the normality of the computed residuals (i.e., those obtained from the retrieved PLSR components) at the 95% confidence level and is computed as

$$JB = \frac{N}{6}[s^2 + \frac{(k-3)^2}{4}], \tag{11}$$

where JB denotes Jarque-Bera statistic, N is the sample size, s is the sample skewness, and k is the sample kurtosis. The Jargue-Bera test is similar to the Lagrange multiplier test and is preferred for large data sets, given the unreliability of other normality tests when the sample size is large. The test matches the skewness and kurtosis of data to examine if it matches a normal distribution of data, be it errors in a regression model or time series data. The significance of the probability values at 95% confidence level was determined by comparing the Jargue-Bera test statistics with the critical value for the test. If Jarque-Bera is large then normality is rejected at $\alpha = 0.05$.

3.3.2. Multi-linear regression analysis

To explore the relationship between TWS changes and precipitation patterns over SA, multi-linear regression analysis (MLRA) was used to model the trends and harmonic components of TWS (mean annual and semi annual amplitudes) of GRACE-derived TWS and precipitation time series. This was achieved through the parameterizations of these components as reported in previous studies (e.g., 63, 74). Trends and harmonic components in the data ($y_{i,j}$) at time (t) were parameterised using the MLRA as (e.g., 74):

$$y_{i,j}(t) = \xi_0 + \xi_1 t + \sum_{i}^{i_{max}} (\xi_{2i} \cos(i\omega t) + \xi_{2i+1} \sin(i\omega t)) + \varepsilon(t), \tag{12}$$

where the least square-estimated coefficients, ξ_0 is an offset, ξ_1, linear trend and ξ_{2i} and ξ_{2i+1} represent the periodic components in the data. The annual amplitude of the data is captured when the period T of the angular frequency $\omega = \frac{2\pi}{T}$ is 12 months with the coefficients, ξ_2 and ξ_3 along with their corresponding trigonometric base functions (i.e., $\cos(\omega t)$ and $\sin(\omega t)$) representing the annual component. The coefficients, ξ_4 and ξ_5 represent the semi-annual component while ε is the error term, which is assumed to be normally distributed. Root mean square errors and coefficients of determination (R^2) were employed to assess the skill of MLRA in modelling TWS and rainfall over South America.

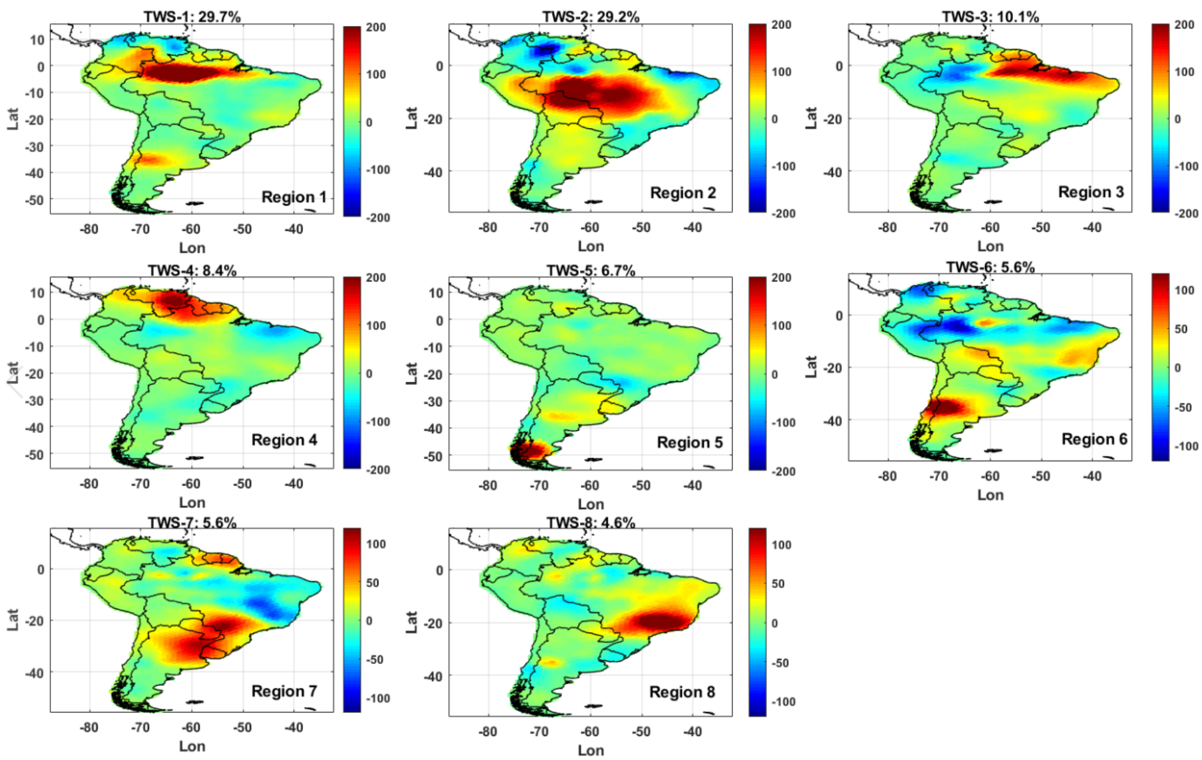

Figure 2: Regionalization of TWS (2002 − 2017) based on pre-orthogonalization and cumulant decomposition methods. The spatial patterns are scaled using the standard deviation of the computed independent components, i.e., the temporal series in Fig. 3. They are also interpreted in conjunction with their corresponding temporal patterns (independent components). The axis labels, latitudes (Lat) and longitudes (Lon) are indicated.

4. Results

4.1. Rotation of terrestrial water storage using higher order statistical algorithms

Other higher order statistical decomposition algorithms, which uses the fixed-point iteration scheme have been employed in filtering satellite gravity signals (32, 33). Contrary to these algorithms, the JADE technique exploits the fourth order cumulants of the data matrix based on remote properties that include non-stationarity, spectral non-Flatness, and non-Gaussianity (e.g., 60, 102, 11, 18). Because of the statistical and numerical efficiency of the JADE approach in solving the optimisation problem (e.g., 102, 12), eight significant independent and well localised spatio-temporal patterns (will be interchangeably designated as 'regions') of TWS were recovered over South America (SA). These patterns highlights considerable inter-annual variability and regional GRACE-hydrological signals over the continent (Fig. 2). The surface water dynamics of the Amazon basin and much of Brazil dominate the independent patterns of TWS in SA (TWS-1 and TWS-2, Fig. 2 and 3) and together account for approximately 60% of the total variability. Region one is localised over the Amazon floodplain (cf. Fig. 1b) and the exchange of water fluxes within this domain is somewhat complex. Apart from the indication that the highest proportion of stored water on the Amazon floodplain comes from the mainstem river, Alsdorf et al. (3) also found that the mainstem discharge was higher compared to the sum of annual water storage and that drained from the Amazon floodplain. Although variations in surface waters represent a considerable component of TWS as observed by GRACE (e.g., 31, 46, 39), the strong exchange of fluxes within the floodplain corridors explains why the dominant patterns of TWS over SA is observed over the Amazon floodplain (TWS-1, Fig. 2 and 3). This is consistent with the results of Frappart et al. (35), who found the strongest spatial loadings of TWS along the Solimões-Amazon corridor and includes the south of the Amazonian and the Negro basins.

In regions three and four (TWS-3 and TWS-4, Figs. 2 and 3), observed GRACE-hydrological signals are annual variations with probable contributions from multi-scale climate oscillations, e.g., El-Ninõ Southern Oscillation (ENSO)-related teleconnections. Some studies found the connections between ENSO and inter-annual TWS variations in these regions (e.g., 65, 50, 70). By further exploring the interplay between ENSO-teleconnections and GRACE-hydrological signals for regions three (northern Brazil) and four (Venezuela), we also found strong evidence that suggests climate teleconnection-driven influence on TWS dynamics. But it is not clear, which hydrological stores or component of GRACE TWS (e.g., surface water, soil moisture, aquifer, etc.) provides this response to climate. The GRACE-hydrological signal in region

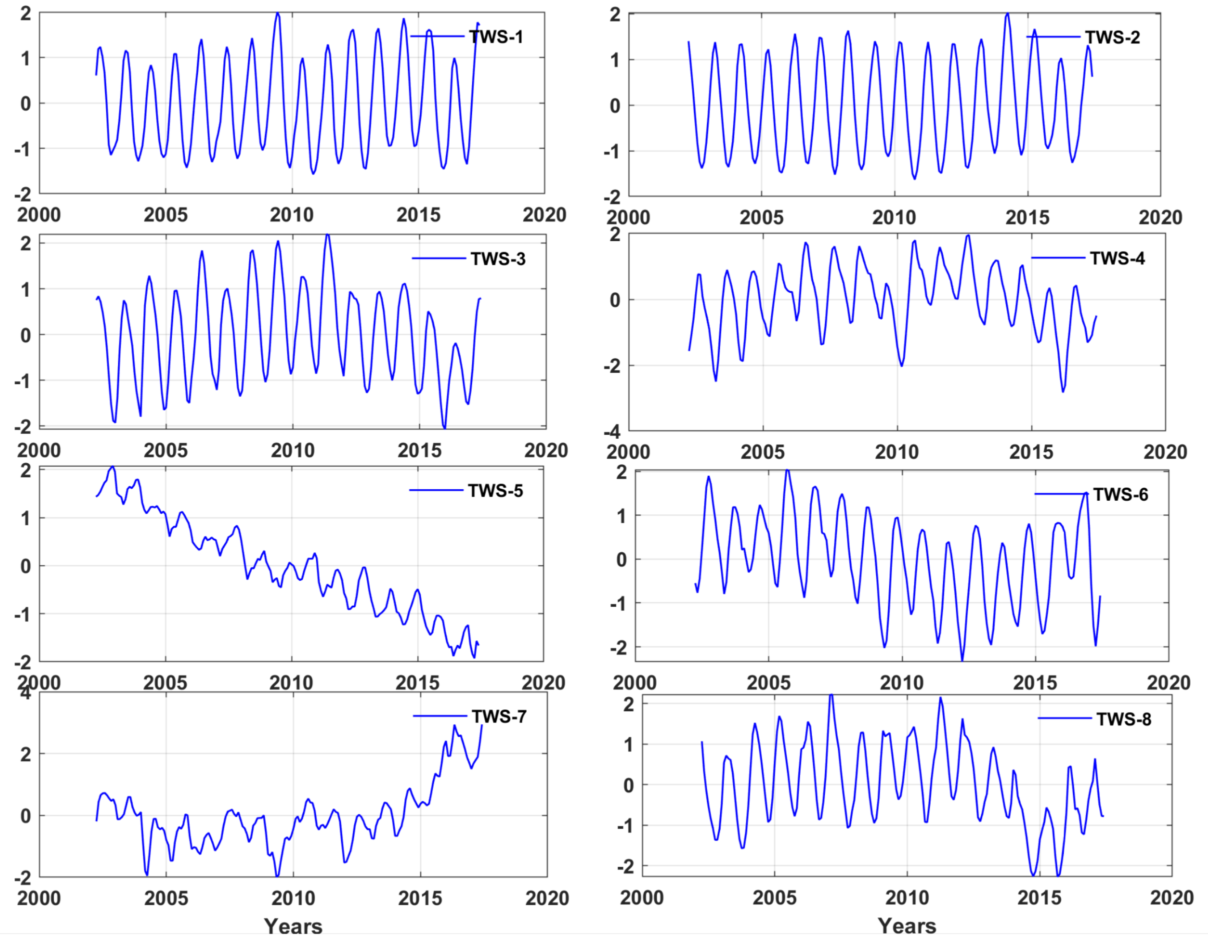

Figure 3: Localised temporal patterns of TWS (2002 – 2017) based on the cumulant decomposition methods similar to Fig. 2. These temporal patterns are in standardised units (y-axis) and correspond to the spatial evolutions and hydrological regions shown in Fig. 2. Amplitudes of TWS for each region (e.g., TWS-1, TWS-2, etc.) are recovered by a joint interpretation of these temporal patterns (in standardised units) with the corresponding spatial patterns in Fig. 2.

five (TWS-5, Figs. 2 and 3) is the melting of the Patagonia ice-field. Consistent with this study, different methods, which includes forward modeling approach have been employed to highlight the continued mass loss in Patagonia (75, 97, 16). This extensive and unabated mass loss in Patagonia ice-field (TWS-5, Fig. 3) is caused by the warming of the climate system, and being the second largest ice body in the Southern Hemisphere, GRACE is a viable tool for the continued monitoring of the impact of rising temperature on Ice fields. Note that similar to the JADE algorithm, estimated negative trends observed over the Patagonia ice-field using the Sen's slope and multi-linear regression model are consistent (Sections 4.2.1 and 4.3.2.

Region six (TWS-6, Figs. 2 and 3) highlights amplitudes of TWS in the Chile region but with most parts falling within Argentina while region seven (TWS-7, Figs. 2 and 3) depicts multi-annual variations in TWS over south Brazil and the neighbouring Central Argentina with a weak opposite phase in north-east Brazil. Having experienced repeated earthquakes, deformations, and other forms of natural disturbances (e.g., 76, 42, 91, 51), the geophysical signals in Chile and the neighbouring Argentina is expected to be dominated and driven by natural and climatic elements. The temporal pattern (TWS-6, Fig. 3) associated with this signal in the Chile/Argentina regions (TWS-6, Fig. 2) show a falling amplitude between 2005 and 2011 while the period after 2011 shows a rising trend, consistent with the results in Section 4.3. Note that region 6 (TWS-6, Fig. 2) also indicates relatively strong opposite TWS

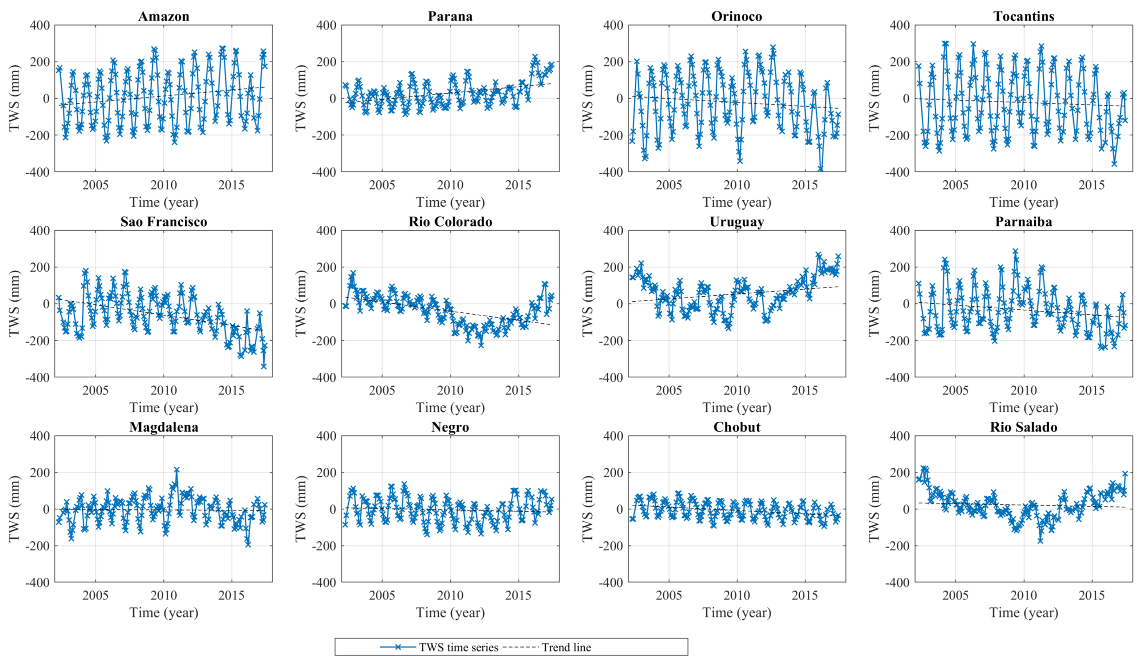

Figure 4: Assessing inter-annual variations of TWS (2002 − 2017) for twelve prominent global river basins in Southern America.

anomalies in the central Amazon basin area and could be related to floodplain and wetland water storage gain between 2005 and 2010, i.e., when jointly interpreted from the corresponding temporal patterns (TWS-6, Fig. 3) and again coincides with numerical results in Section 4.3. The argument here is that elevation of the flood plains of Amazon basin (low elevation areas less than 200 m above mean sea level) coincides with the unique features of TWS for region 6 (e.g., the region with the most freshwater-Fig. 1) as depicted in its spatial patterns (TWS-6, Fig. 2). That is, the spatial patterns with positive loadings in Chile and environ (TWS-6, Fig. 2) are interpreted as wet conditions (or gain in surface mass) if multiplied with its corresponding positive amplitudes in Fig. 3. Similarly, the spatial patterns with negative loadings in Fig. 2 (Amazon region) are interpreted as wet conditions (or rise in surface mass) if multiplied with its corresponding negative amplitudes (TWS-6, Fig. 3). The low elevation areas of the Amazon and the strong annual fluctuations (TWS-6, Fig. 3) suggests that it appears to be a rather permanent wetland water storage induced by rainfall seasonality (cf. Fig. 1). As opposed to the high elevation areas of Chile (greater than 3500 m above mean sea level), which shows annual fluctuations in TWS, it can be argued that elevation plays a role in the Amazon flood plain wetland water storage. Notably, this Amazon signal (region 6) is different from regions 1 and 2 where river storage, exchange of fluxes between tributaries, including vertical movement of shallow groundwater could be major drivers of GRACE-derived TWS variations along the Amazon corridor.

Regarding the spatial patterns in region 7 (TWS-7, Fig. 2), the strongest signals with opposite phase occur within southern Brazil. The corresponding time series (TWS-7, Fig. 3) show relatively strong negative anomalies in 2004 and 2009 before the strong rise that occurred after 2010. The peak negative anomalies in 2004 and 2009 appear to coincide with severe droughts in the region, especially the summer drought of 2004/2005. As highlighted further in Section 4.2.1, the short term trends in TWS and rainfall during this period around this region $(2012-2017)$ show consistency between 2012 and 2014 but with small dissimilarity during the $2010-2012$ period and can be explored further in future studies that focus on this region. Region eight (TWS-8, Figs. 2 and 3) is the GRACE-hydrological signal native to north-east Brazil (e.g., 84). The declining trend in TWS during the $2011-2015$ period and the strongest negative anomaly observed between 2014 and 2015 (TWS-8, Fig. 3) coincide with the widely reported super extreme droughts that ravaged most eastern sections of Brazil during the same period, especially 2015 (e.g., 27, 103, 36). This prolonged drought, which occurred in much of north-east Brazil during most of the 2010–2013 period, resulting in considerable declines in TWS (TWS-8, Fig. 3) triggered the need to improve drought-related policy and management strategies at various levels of government Brazil (see, 38). Owing to limited annual rainfall, north-east Brazil is generally a water deficit region and depends on surface water from the Amazon basin for irrigation and hydropower generation. The Sao Francisco river basin in Brazil depends on water transfers between river basins. Moreover, the National Water Agency of Brazil reported in 2015 that 79% of total water withdrawn was for irrigated agriculture. Hence, GRACE is a viable hydrological tool to support the monitoring of hydrological drought and its impacts on water availability and human abstraction (see, 27).

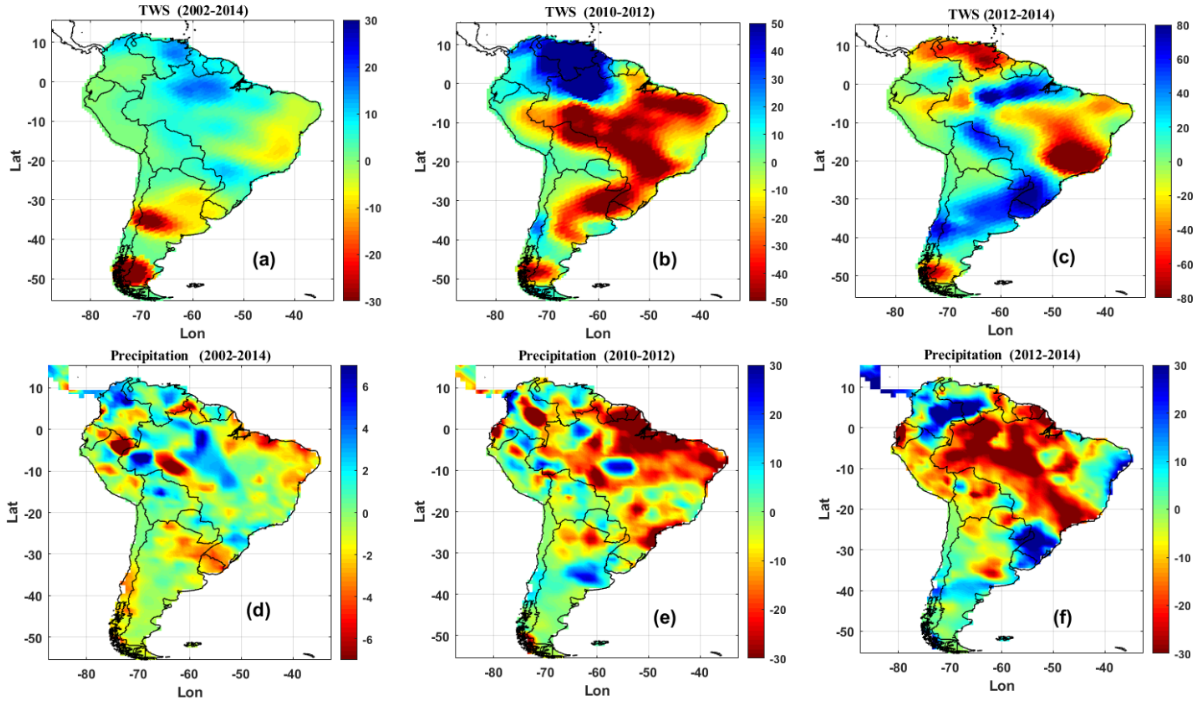

Figure 5: Spatial distribution of trends in TWS (a-c) and precipitation (d-f) for three different periods (2002 – 2014, 2010 – 2012, and 2012 – 2014). All units are in mm/year.

4.2. Assessing inter-annual variations and changes in TWS

In this section, results for the region-specific (twelve river basins) estimates of linear rates in TWS are highlighted. These river basins are among the well known global river basins. Add to this, time series of TWS grids are compared to those of rainfall over SA based on cross-correlograms.

4.2.1. Recent changes in TWS in South American river basins

Observed temporal variations in the 15-year GRACE-derived TWS over 12 river basins are marked with strong fluctuations. With an estimated linear rate of -11.29 ± 1.71 mm/yr, Sao Francisco showed the strongest fall while Parana indicated the strongest rise (6.88 ± 1.13 mm/yr) in TWS during the $2002-2017$ period (Fig. 4). The summary of Mann-Kendall's test statistics for all significant ($\alpha = 0.05$) linear trends observed in the 12 river basins for the two periods (2002 – 2017 and 2010 – 2017) analysed are highlighted in Table 1. Considering the estimated linear rates between 2010 and 2017, the strongest decline (-38.48 ± 7.90 mm/yr) in TWS was found in Orinoco while Uruguay showed a considerable increase in TWS (28.28 ± 3.49 mm/yr) unlike other basins (Fig. 4 and Table 1). During the same period (2010 – 2017), significant increase in TWS were also observed in Parana (17.92 ± 3.44 mm/yr), Rio Colorado

Table 1: Estimated trends in temporal variations of TWS for 12 river basins in South America during the $2002-2017$ and $2010-2017$ periods. The null hypothesis (no significant trend), H_0, was tested at $\alpha = 0.05$ (95% confidence level) using the Mann-Kendall's statistics. The p-value (probability threshold agreed for the significance level) and root mean square error are indicated. Note, the trends with asterisks (*) are not statistically significant.

	River basins	2002/04 – 2017/06			2010/04 – 2017/06		
S/N		Trend (mm/yr)	p-value	RMSE	Trend (mm/yr)	p-value	RMSE
1	Amazon	6.54 ±2.60	0.004	141.755	*11.06 ±8.49	0.221	151.317
2	Parana	6.88 ±1.13	0.000	61.441	17.92 ±3.44	0.000	61.29
3	Orinoco	*-4.25 ±2.89	0.096	157.598	-38.48 ±7.90	0.000	142.128
4	Tocantins	*-2.60 ±3.06	0.5186	166.345	*-16.65 ±8.98	0.265	160.039
5	Sao Francisco	-11.29 ±1.71	0.000	93.126	-30.84 ±4.17	0.000	74.30
6	Rio Colorado	-9.91 ±1.22	0.000	66.437	23.99 ±2.60	0.000	46.377
7	Uruguay	5.33 ±1.54	0.000	83.982	28.28 ±3.49	0.000	62.13
8	Parnaiba	-5.38 ±2.05	0.0108	111.733	-24.42 ±4.95	0.000	88.151
9	Magdalena	*-0.44 ±1.25	0.925	68.134	-18.76 ±3.58	0.000	63.86
10	Negro	*-1.51 ±1.20	0.1699	65.124	13.0 ±3.27	0.000	58.268
11	Chobut	-3.74 ±0.78	0.000	42.578	*-4.17 ±2.30	0.011	41.068
12	Rio Salado	*-1.49 ±1.31	0.1671	71.137	25.17 ±2.78	0.000	49.611

(23.99±2.60 mm/yr), Negro (13.0±3.27 mm/yr), and Rio Salado (25.17±2.78 mm/yr) while Sao Francisco (-30.84±4.17) and Parnaiba (-24.42±4.95) indicated relatively strong negative trends in TWS (Fig. 4 and Table 1).

The spatial distribution of trends in TWS and precipitation over South America suggest complex hydrological structures and processes. For instance, the long term declines in TWS over Chile/Argentina regions and melting of the Patagonia ice field are inconsistent with rainfall (Figs. 5a and d). This is because the factors driving the hydrology of these areas are beyond rainfall. Recall that these signals coincide with the spatial and temporal patterns in regions five and six (TWS-5 and TWS-6, Figs. 2 and 3) and further highlights the effectiveness of the JADE rotation in localizing geophysical signals. Further, the analyses of short term trends ($2010-2012$ and $2012-2014$) also highlights the remarkable difference in recent changes in TWS in relation to rainfall. Such inconsistencies are mostly observed over Venezuela, Brazil, and Argentina (Figs. 5b-c and e-f). However, the TWS trends in Northeast Brazil between 2012 and 2014 are consistent with those of rainfall (Figs. 5e and f). Whereas TWS in some regions in SA respond to changes in rainfall and climatic conditions as is the case in north east and southern Brazil (Figs. 5b-c and e-f), the complex hydrogeological structures in some areas may trigger interesting hydrological processes. To understands this processes, the grid based TWS-rainfall association and phase lags during the entire period are explored in the next section by implementing a cross-correlation.

4.2.2. GRACE TWS vs rainfall

To explore the TWS-rainfall relationship, cross-correlation between detrended series of GRACE-TWS and GPCC-rainfall was analysed. From the water budget equation, TWS changes in time. In other words, observed changes in TWS balances precipitation minus evaporation and runoff. Figure 6 shows the lags (presented as colored surface) at which the two series present the maximum correlation coefficients (presented as contour lines). Overall, rainfall rates lead TWS in approximately zero to three months for almost all of SA with correlation coefficient ranging from approximately 0.60 to 0.80 (Fig. 6). For example, considering the physiographic regions of SA, the Brazilian Highlands, the Amazon Rainforest, and the Gran Chaco regions (spreads across eastern Bolivia, western Paraguay, northern Argentina and sections of Brazil) all indicate relatively high correlations with rainfall leading TWS. Moreover, the Lianos and Guiana Highlands (both at northern SA), and the Andes Mountains (apart from the portion that surrounds the Altiplano and Atacama Desert) present good phase agreement with high correlation coefficients. While this shows good feedback of TWS on rainfall for almost all SA, the relationship between TWS and rainfall during the period is statistically not significant at the 95% confidence interval.

However, there are exceptions in the regions below latitude 16°, which are arid regions characterized by relatively low precipitation rates (Fig. 1b). The Chile coastline and the Patagonia are regions where correlations are modest ranging from 0.40 to 0.60 and rainfall generally leads TWS with a phase greater than four months (Fig. 6). There are also some hydrological hot spots (regions below latitude 16 °) with TWS leading rainfall with a phase of 12 months but with high correlation only for the Lake Titicaca region (cf. Fig. 1 and 6). But around the Patagonian region and Chobut, Colorado and Salgado basins, correlation coefficients between the series are low ($r = 0.40$) indicating that the key driver of variations in TWS is beyond rainfall. For example, the Pampas of Argentina (approximately between latitudes 40°S to 32°S and longitudes 56°W to 64°W) is characterized by annual precipitations of 500 − 1000 mm (Fig. 1b). TWS shows relatively low annual peaks with a negative linear trends of -5 to -15 mm/yr of mass loss. This could be attributed to changes in the land use

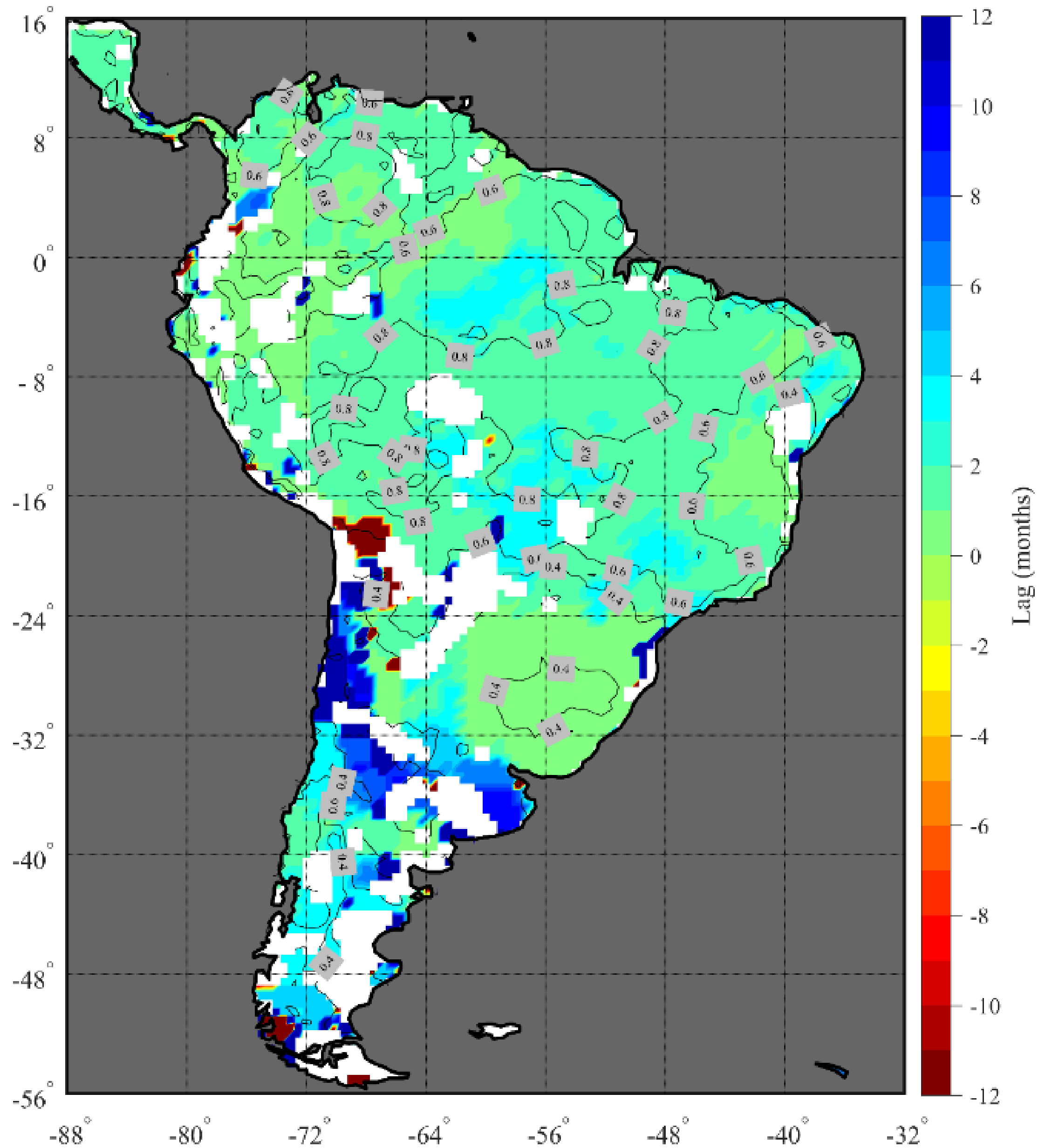

Figure 6: Correlation analysis showing phase lags at which maximum correlation coefficients occurred for TWS versus rainfall during a common period $(2002 - 2017)$. The contour lines show the correlation coefficients while the values depicted in the color bar indicate the lags in months. Regarding lags, negative values mean TWS leads rainfall while positive values imply rainfall leads TWS. Only statistically significant correlations ($\alpha = 0.05$) are presented.

due to the crop rotations or natural vegetation, which might decrease groundwater recharge and thus decrease TWS storages (e.g., 48). This is particularly true for Patagonia since it is characteristically a dry climate. As shown in region 6 (Figs. 2 and Fig. 3), the Patagonia ice fields are undergoing a contemporary melting and retreating of glacial ice and is consistent with previous studies (e.g., 97, 16). The Andean Plateau (Altiplano) presents a phase lead greater than twelve months for rainfall relative to TWS series and includes part of the Pampas region. Furthermore, part of the Pampas region (southern) also shows a phase lead of about 12 months (TWS lags rainfall). In both cases, we found that correlation coefficients were low, mostly between around 0.10 and 0.20 and insignificant.

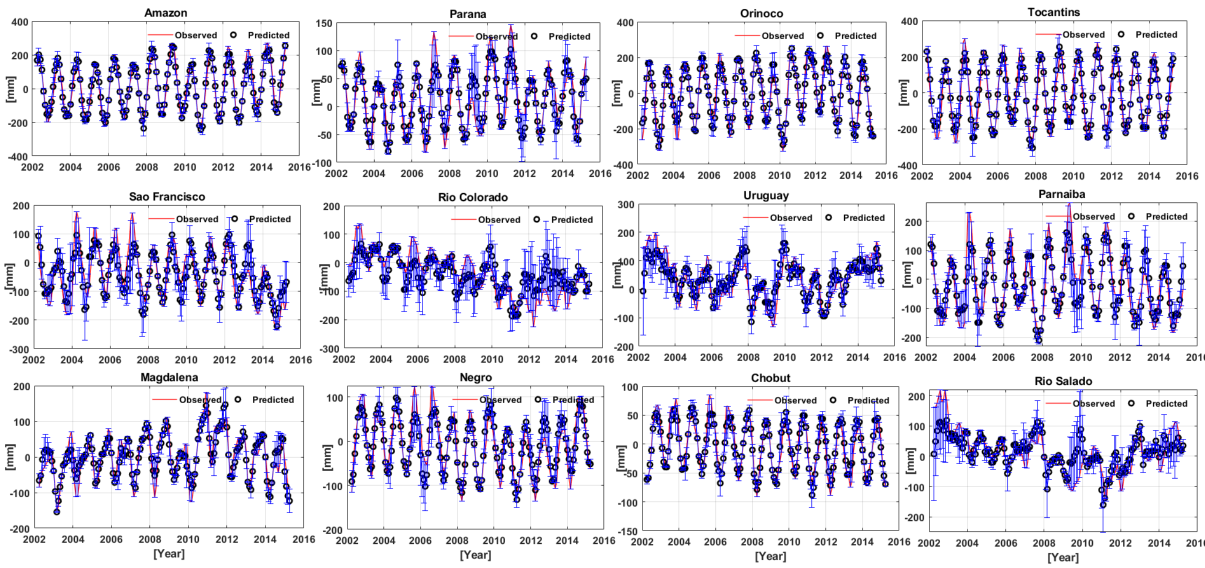

Figure 7: Modelling GRACE-derived TWS (2002 – 2017) using the PLSR model. Temporal patterns of predicted and observed TWS for the 12 prominent river basins in Fig. 5 are compared using several validation metrics.

4.3. Modelling TWS using parameter estimation techniques

4.3.1. Partial least square regression prediction of river basin TWS

Overall, the temporal variations of TWS are well predicted for most of the river basins (Fig. 7) and show reasonable residuals and considerable association with observed TWS based on three validation metrics used (Figs. 8a-b). In terms of the performance of PLSR model, time series of TWS in the Amazon, Orinoco Tocantins, and Chobut basins were well predicted and showed optimum skills based on these validation metrics (R^2, IA, and NSE). These basins indicated R^2, IA, and NSE coefficients above 0.83 (Fig. 8b) but with Chobut having the least residual and RMSE (Fig. 8a). However, Rio Colorado, Rio Salado, Uruguay, Sao Francisco, and Parnaiba indicated relatively higher TWS residuals and RMSEs (Figs. 7 and 8a). The uncertainties (i.e., residuals and RMSEs) in predicted time series of TWS in these locations were also reflected in their observed validation metrics with Rio Colorado showing the lowest R^2 (0.49), IA (0.66), and NSE (0.49) (Fig. 8b). The obvious poor performance of the PLSR model

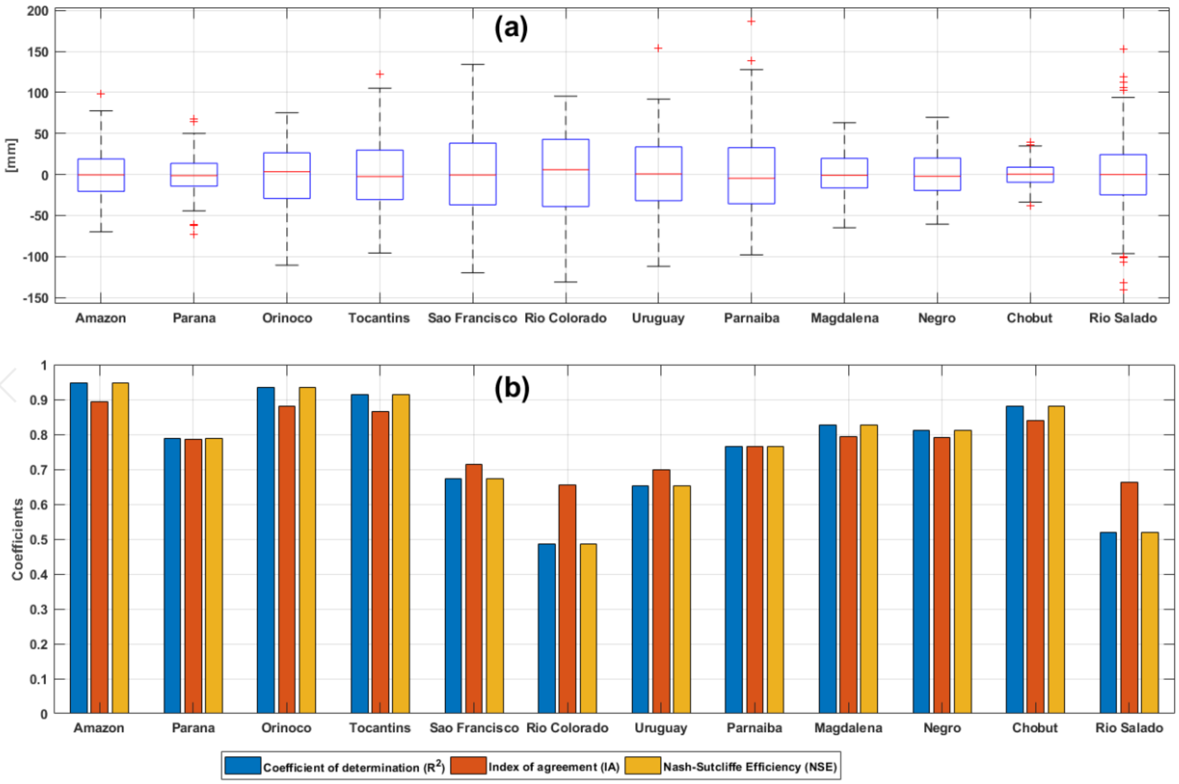

Figure 8: Analysis of PLSR model outputs for TWS in South American river basins.(a) Uncertainties in the PLSR model prediction of TWS over the 12 river basins for 157 time steps (2002/04 – 2015/04). The TWS residuals (i.e., the difference between the predicted and observed obtained in mm) indicated here are for PLSR calibration based on nine significant components. (b) Performance of PLSR model in predicting TWS in the 12 river basins based on three skill metrics (coefficient of determination (R^2), Index of Agreement (IA), Nash-Sutcliffe Efficiency (NSE)).

in Rio Colorado, Rio Salado, and Sao Francisco (Fig. 8a and b) gives credence to the argument of the perceived contributions of non-climatic elements to observed inter-annual variations in TWS. Especially for the basins located in Brazil (e.g., Sao Francisco), Uruguay, and Argentina, the TWS-rainfall relationship as was highlighted in Section 4.2.2 indicated poor association with considerable phase lags in most catchments. This may not be unconnected with human water management as Getirana (36), for example, found considerable correlations of monthly time series of TWSA and ground-based water storage observations with most reservoirs within southeastern Brazil. Given the observed residuals and the index of agreement (Figs. 7 and 8a), it seems the predictability of TWS based on hydro-climatic variables could be challenging in some river basins of SA. As indicated in Fig. 6, some of these regions (Andean Plateau, Pampas, etc.) showed low correlation values ranging from 0.00 to 0.20 and with more than 12 months in phase lag between.

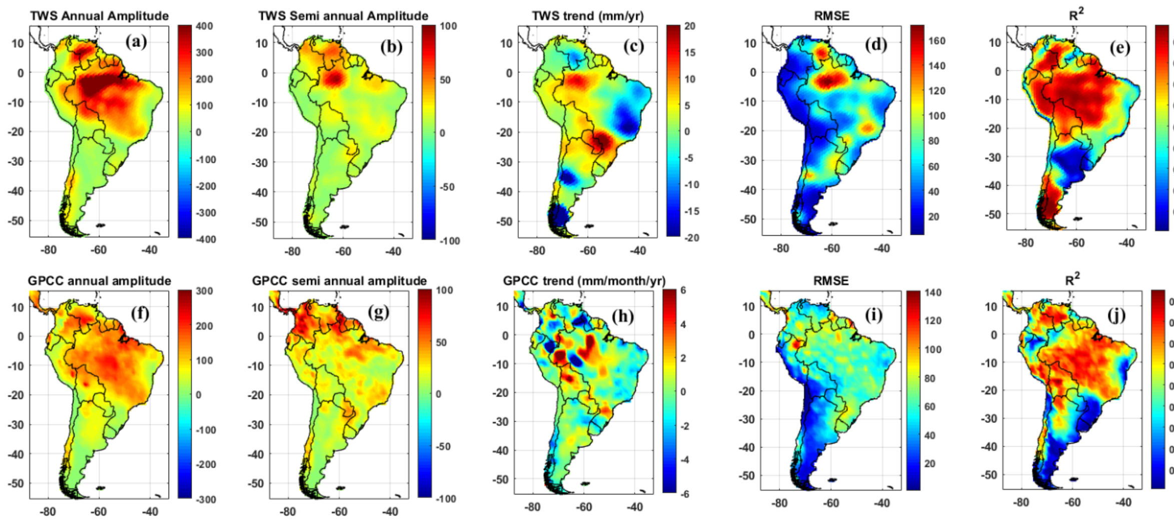

Figure 9: Modelling (a-e) GRACE-derived TWS and (f-j) GPCC precipitation using the multi-linear regression formulation during the period $2002 - 2017$.

4.3.2. Multi-linear regression of TWS grids

In this section, the results of simulated TWS and rainfall grids over SA using the MLRA technique are highlighted. The mean annual amplitudes of rainfall observed over the Amazon basin area is consistent with TWS (Figs. 9a and f) while the trends and mean semi-annual amplitudes of TWS show significant disparity and does not completely mimic the modelled patterns of rainfall (Figs. 9b-c and g-h). As opposed to rainfall, the only spot with considerable semi-annual signal is in the Brazil section of the Amazon basin (Figs. 9b and g). The dissimilarity in trends (TWS and rainfall), especially those observed in Brazil and Argentina (Figs. 9c and h) confirm the complex geophysical processes in the continent as highlighted in previous sections. Overall, the root mean square error (RMSE) is relatively low over the arid regions of SA for rainfall and TWS but somewhat higher for TWS in the central Amazon basin (Figs. 9d and i). Such relatively high uncertainties may result from the influence of important processes of inter-annual variability (e.g., Pacific Decadal Oscillation) or the complex properties of the Amazon floodplain as it relates to exchange of fluxes and water storage (e.g., 3). However, the coefficient of determination (R^2) suggest the model predicts variations in TWS and rainfall quite well with R^2 values ranging from 1.00 to 0.80 (Figs. 9e and j). Except for R^2 values (i.e., TWS) over Patagonia (Figs. 9e), the regions that are poorly simulated in the two products are generally found below Latitude 20° (Figs. 9e and j). The low R^2 values in TWS for example, could imply strong interactions with non-climatic factors and/or the multi-linear regression model is not suitable for those locations. Overall, the modelling of TWS and rainfall over the Amazon basin show a good fit and suggest it can be predicted quite well. This is justified by the result in Section 4.2.2 where the TWS-rainfall relationship around the Brazilian highlands and much of the Amazon rainforest is relatively high with rainfall leading TWS. But the plenitude of observed R^2 ranging from 0 to 0.30 in some regions of the continent could imply the predominant influence of other hydrological drivers, e.g., natural disturbances and perturbations of multi-scale global climate signals. The influence of the latter on TWS in tropical SA has been reported (e.g., 50) while the contributions of the former to changes in TWS in the Chile/Argentina regions have been affirmed in some studies (e.g., 75, 40).

5. Discussion

5.1. Assessing drivers of land water storage

Global climate is changing. The impacts of such changes, which have been attributed to rising anthropogenic emissions of greenhouse gases, amongst other things are evident in natural systems and acceleration of the water cycle, be it at regional or global scales. The rise in global sea levels, long-term declines in rainfall and TWS, and increased frequency in flood and drought events (e.g., 75, 83, 67, 9, 69, 90, 81) across the globe are some apparent indices of a changing global climate. As with other regions whose TWS variations and discharge are largely rainfall-dependent (e.g., 59, 58, 70, 19), land water storage dynamics (includes river discharge and surface runoff) in SA are arguably driven by changes in climate and other key processes of inter-annual variability such as ENSO (e.g., 50, 21, 34, 35). Incessant extreme droughts event in South America, for instance, have been linked to large scale variations in the tropical oceans (Pacific and Atlantic). This was recently echoed by Erfanian et al. (23) who also found significant relationship between unparalleled drought events in South America and extreme anomalies in SST of the nearby oceans. Whereas inter-annual changes in rainfall over tropical ecosystems are significantly modulated by the tropical oceans (64, 68, 79, 66), our results in Section 4.1 confirm that these drought episodes have considerable impacts on TWS. This is true for Brazil where the observed decline in TWS between 2012 and 2015 (TWS-8, Figs. 2, 3; and 5) coincided with the extreme drought that ravaged Brazil during the period (e.g., 27). Apart from the continued mass loss in Patagonia (TWS-5, Figs. 2 and 3) caused by climate warming, the observed TWS-rainfall relationship (Section 4.2) also highlights the importance of climate variability in observed variations in TWS over most sub-regions of SA. Within the context of TWS response to climate variability induced rainfall, there are indications however, that some hydrological signals are not unconnected with non-climatic influence.

In practical geodetic concepts as it relates to mass redistributions caused by changes in gravity fields, Chile (TWS-6, Figs. 2 and 3) is one of the most complex hydrological regions in SA (28). Because of its hydro-geodetic characteristics and geophysical formation, the Chilean region and environ, for example, are vulnerable to vertical deformations, seismicity, and earthquakes. (see, e.g., 55, 54, 42). Some of these geodetic perturbations and disturbances as also found in other regions (e.g., 17), have enduring hydro-ecological effects on the environments (e.g., 42). Hydrologically, they leave behind extraneous geophysical signals that become available as an integral part of observed hydrological changes in such regions. These signals complicate our understanding of land water storage drivers. For example, in the Chile earthquake of 27 February 2010, Han et al. (40) found a gravity anomaly of -5μGal with a spatial scale of 500 km east of the epicenter after the earthquake. If we consider the relation between water storage change (Δh, in meters) and gravitational attraction due to the water mass (Δg_{TWS}, m/s^2) as: $\Delta g_{\text{TWS}} \approx 4.2 \cdot s_y \cdot \Delta h$, the change in gravity due to the Maule event of -5×10^{-8} m/s^2 would be equivalent to an apparent change in TWS of about -39 mm considering s_y, the specific yield (dimensionless), equals 0.3. Correcting the impacts of this gravity shift on the overall surface mass changes around the region is a complex geodetic problem and this was not address in this study since it is a localized effect.

Since the inception of GRACE, there have been at least four earthquakes (e.g., 2010(Mw=8.8), 2014(Mw=8.2), 2015(Mw=8.3), and 2016(Mw=7.6)) and other geodetic disturbances, e.g., tsunamis and volcanism in Chile (e.g., 76, 42, 55, 54, 91, 16). While Han et al. (40) found strong gravity shift after the 2010 Chile earthquake, which affected gravity anomalies in Argentina, the observed TWS trend in Central Argentina was partly attributed to this magnitude-8.8 earthquake, in addition to natural drivers such as rainfall (75). It is obvious that the GRACE hydrological time series in Fig. 3 are mostly dominated by strong inter-annual variations. But when the trends, annual and semi annual amplitudes of TWS were isolated using a multi-linear regression parameterisation, region 6 (TWS-6, Fig. 3) showed a considerable rise in TWS after 2011 when it was statistically decomposed (not shown). This rise in TWS could be artificial jumps in surface mass variations related to post seismic deformations or coseismic jump in the geoid (54).

Based on the PLSR model, TWS in Sao Francisco, Rio Colorado and Rio Salado showed less association with climatic parameters. This association results probably from a combined influence of human water management practices and other complex environmental conditions and processes mentioned earlier. For instance, In the Sao Francisco river basin in South America, for example, about 44 million people depend on water transfers between river basins. Further, the National Water Agency of Brazil reported in 2015 that 79% of total water withdrawn was for irrigated agriculture. This kind of footprints and perhaps those caused by geodetic perturbations could leave behind surface mass variations that can be misconstrued or interpreted as those induced by rainfall seasonality. Also, water-limited regions in Brazil mostly coincide with semi-arid areas and those with fractured aquifers were there is heavy reliance on surface waters (4). The linear trend observed in water-limited basins such as Sao Francisco (-30.84 ± 4.17 mm/yr) between 2010 and 2017 in Brazil shows a considerable fall (Table 1) and could result in a rise in water demand, especially in the light of unprecedented changes in rainfall. With a total of 19,361 man-made reservoirs as at 2016, Brazil apparently shows increased dependence on surface water resources for irrigation and hydropower with Sao Francisco being one of the major hotspots for surface water consumption (4). Hence, this obvious anthropogenic footprint in the region is expected to impact the prediction of TWS variations.

5.2. Predicting land water storage

For an optimal prediction of TWS (response or dependent variables) over each river basin, a two-step regularization approach that combined JADE method and PLSR was employed. Fourteen independent components of SST anomalies (i.e., seven independent components each from the Pacific and Atlantic oceans), i.e., (independent variables) obtained from the combined PCA-cumulant decomposition were used in the PLSR model to predict TWS. A subset of the latent variables based on nine PLSR components were retrieved and used to develop a prediction model. The observed PLSR model uncertainties (Fig. 8) in the simulation of river basin TWS using the leading independent SST modes from the Pacific and Atlantic oceans for some regions (e.g., Amazon, Orinoco, Tocantins, etc.) suggest the considerable role of climate variability in long-term changes in river basin TWS. However, the PLSR model was somewhat less effective in other river basins (Rio Salado, Sao Francisco, Rio Colorado, and Uruguay) given their modest skills (R^2, IA, and NSE; Fig. 8b) and relatively high RSMEs (not shown). The Jarque-Bera statistical test for these basins (p =0.5, 0.1, 0.2, 0.5, 0.39 for Sao Francisco, Rio Colorado, Uruguay, and Rio Salado, respectively) indicated the model's estimated residuals were not normally distributed as their probability values were greater than the 0.05 confidence level. The modest predictive capacity of TWS using climate components as exhibited by the PLSR scheme in these basins merely imply that TWS are significantly driven by non-climatic factors as we have unpacked in previous sections. The increasing dynamics in global TWS owing to the combined influence of climate and other stressors restricts other conventional models (e.g., least squares) in predictive frameworks. Although it bears some similarity to principal component analysis, i.e., in terms of seeking a hyperplane that maximizes the variance of the input variable (71), one key advantage of the PLSR model is that it mitigates the effect of multi-collinearity (e.g., 8, 49, 99) by ensuring that only significant components relevant to the response variable are retained for the regression. Although the orthogonality of the principal components apparently also solves this multi-collinearity problem, the choice of an optimum subset of predictors however, remains a key issue (e.g., 49, 99). The PLSR scheme addresses this problem, thus making it more suitable in the forecast of hydrological quantities such as GRACE-derived TWS. This innate potential of the PLSR model is what we have explored in this study for the prediction of river basin TWS in South America for the first time and complements existing frameworks of other statistical predictive models deployed recently for routine analysis and modelling of climatic variables (61, 47, 8).

Considering the low R^2 values in modelled TWS, optimising the multi-linear regression model for improved freshwater prediction could imply an expansion of the independent variables. Unlike other regions where variations in rivers, lakes, and floodplains do not contribute to observed changes in GRACE-TWS (37), TWS over the Amazon basin is considerably driven mostly by its surface waters (rivers and estuaries) along the floodplain. The dominant patterns of TWS observed over the Amazon basin in this study aligns with an earlier report by Kim et al. (46) who found that river storage and sub-surface flow accounted for about 73% of TWS variations in Amazon. As opposed to the Amazon region, significant large scale alteration of hydrological processes resulting from multiple strings of human activities, e.g., surface water developments and water diversion in other large watersheds are well known drivers of surface water hydrology (e.g., 61, 93). Hence, independent variables, e.g., river discharge and evapotranspiration are critical water budget quantities expected to improve freshwater prediction for the Amazon basin, in addition to accounting for climate teleconnection-driven rainfall.

However, accounting for human-induced influence (e.g., surface water developments and increased water abstraction) in predictive models is challenging and may require advance statistical approaches. For instance, in the light of the observed strong gravimetric contributions of Lake Volta to GRACE-derived TWS over the Volta basin, a weighted least squares formulation of global spherical harmonic analysis was integrated with a fourth-order cumulant statistics to isolate non-climatic hydrological time series of surface water storage (see, 62). By recovering this surface water contributions caused by human water management strategies, TWS over the Volta basin can be predicted more accurately. Research problems that seek to quantify the impacts of anthropogenic contributions on regional or continental hydrology are new innovative directions that will support predictive frameworks and effective characterisation of key hydrologic metrics.

6. Conclusion

The knowledge of global freshwater response to critical stressors, e.g., human water abstraction is crucial to improving predictive frameworks that support water governance and management schemes. Hence, an innovative approach that combined JADE (Joint Approximate Diagonalisation of Eigen matrices) algorithm and partial least square regression was employed in this study to assess GRACE-derived terrestrial water storage (TWS) over South America (SA). The temporal evolutions of TWS over prominent river basins in the continent was also predicted using independent patterns of sea surface temperature (SST) anomalies of the nearby oceans. The conclusions from this study are summarised as follows:

(i) GRACE-hydrological signals within the Amazon basin and much of Brazil dominate the independent patterns of TWS in SA and together account for approximately 60% of the total variability. The strong exchange of fluxes within the floodplain corridors of the Amazon and the influence of climate modes explain why strong spatial patterns of TWS is observed over the Amazon basin and the entire tropical SA. Amongst other geophysical signals identified, the JADE rotation of TWS over SA isolated the extensive and unabated mass loss in Patagonia ice-field caused by the warming of the climate system. Still on the JADE rotation of TWS, we noted that the GRACE-hydrological signals native to north-east Brazil are largely associated with extreme hydro-climatic events (droughts).

(ii) Having experienced repeated earthquakes, seismicity, deformations, and other forms of natural disturbances, the geophysical signals in Chile and the neighbouring Argentina are expected to be dominated and driven by both dynamical physical processes and climatic elements. Because of this complex hydro-geodetic structure and geophysical formation, interpreting GRACE-hydrological signals in these regions is challenging and requires caution.

(iii) Estimated TWS trends ($\alpha = 0.05$) in the twelve river basins in SA for the $2010 - 2017$ period indicates Orinoco had the strongest fall (-38.48 ± 7.90 mm/yr) in TWS while

Uruguay showed a considerable rise (28.28±3.49 mm/yr) unlike other basins. During this same period ($2010 - 2017$), relatively strong increase in TWS was also observed in Rio Colorado (23.99±2.60 mm/yr) and Rio Salado (25.17±2.78 mm/yr) while Sao Francisco (−30.84±4.17) and Parnaiba (−24.42±4.95) indicated relatively strong negative trends in TWS. Generally, the grid-based comparisons of rainfall and TWS trends over some areas of SA are inconsistent and suggests that the hydrological drivers of these regions (e.g., Patagonia, Brazil, Argentina, and Venezuela) are beyond rainfall.

(iv) Overall, rainfall leads TWS in approximately one to three months in much of SA with maximum correlation coefficients (r) ranging from approximately 0.6 to 0.8, especially around Brazil and the Amazon basin. TWS in some regions however, show low and modest correlations with rainfall. In these hydrological regions, rainfall leads TWS with a phase lag ranging from $2 - 4$ months and indicate that apart from rainfall other key drivers of variations in TWS exists since, for example, such regions are typically characterised by a dry climate. Similar conclusion applies to some hot spots in the semi-arid north-east Brazil, where the TWS-rainfall association is poor and not significant during the period.

(v) Based on several skill metrics and the Jarque-Bera statistical test for the PLSR model output, TWS in Sao Francisco, Rio Colorado and Rio Salado showed less association with climatic parameters. This association could be the result of a combined influence of human water management practices and other complex environmental conditions and processes. The roles of reservoir storage and dams on surface hydrology, for example, in Sao Francisco where water abstraction for irrigation is nearly 80% require further investigation. Considering the low R^2 values and uncertainties in modelled TWS over SA in some hydrological regions, optimising the multi-linear regression model for improved freshwater prediction could imply an expansion of the independent variables to include other relevant important physical processes.

Acknowledgments

The authors are grateful to NASA and NOAA for all the data used in this study. We thank the Editor and three anonymous reviewers whose constructive comments helped in improving the content and quality of this article. Vagner G. Ferreira acknowledges the support from the National Natural Science Foundation of China (Grant No. 41574001) and the Fundamental Research Funds for the Central Universities (Grant No. 2015B21014).

References

[1] Agutu, N., Awange, J., Zerihun, A., Ndehedehe, C., Kuhn, M., and Fukuda, Y. (2017). Assessing multi-satellite remote sensing, reanalysis, and land surface models' products in characterizing agricultural drought in East Africa. *Remote Sensing of Environment*, 194(0):287–302. doi:10.1016/j.rse.2017.03.041.

[2] Ahmed, M., Sultan, M., J.Wahr, and Yan, E. (2014). The use of GRACE data to monitor natural and anthropogenic induced variations in water availability across Africa. *Earth Science Reviews*, 136:289–300. doi:10.1016/j.earscirev.2014.05.009.

[3] Alsdorf, D., Han, S.-C., Bates, P., and Melack, J. (2010). Seasonal water storage on the amazon floodplain measured from satellites. *Remote Sensing of Environment*, 114(11):2448 – 2456. doi:10.1016/j.rse.2010.05.020.

[4] ANA (2017). Brazilian water resources report 2017. *National Water Agenccy*.

[5] Andam-Akorful, S., Ferreira, V., Ndehedehe, C. E., and Quaye-Ballard, J. (2017). An investigation into the freshwater variability in West Africa during $1979-2010$. *International Journal of Climatology*, 37(S1):333–349. doi:10.1002/joc.5006.

[6] Anyah, R., Forootan, E., Awange, J., and Khaki, M. (2018). Understanding linkages between global climate indices and terrestrial water storage changes over africa using GRACE products. *Science of The Total Environment*, 635:1405 – 1416. doi:10.1016/j.scitotenv.2018.04.159.

[7] Awange, J., Fleming, K., Kuhn, M., Featherstone, W., Heck, B., and Anjasmara, I. (2011). On the suitability of the $4°\times4°$ GRACE mascon solutions for remote sensing Australian hydrology. *Remote Sensing of Environment*, 115(3):864 – 875. doi:10.1016/j.rse.2010.11.014.

[8] Biswas, H. R. and Kundu, P. K. (2018). A principal component analysis based model to predict post-monsoon tropical cyclone activity in the Bay of Bengal using oceanic Niño index and dipole mode index. *International Journal of Climatology*, 38(5):2415–2422. doi:10.1002/joc.5344.

[9] Boening, C., Willis, J. K., Landerer, F. W., Nerem, R. S., and Fasullo, J. (2012). The 2011 La Niña: So strong, the oceans fell. *Geophysical Research Letters*, 39(19):L19602. doi:10.1029/2012GL053055.

[10] Cardoso, J.-F. (1991). Super-symmetric decomposition of the fourth-order cumulant tensor, blind identification of more sources than sensors. Retrieved from:http://perso.telecom-paristech.fr/ cardoso/Papers.PDF/icassp91.pdf. Accessed 15 January 2016.

[11] Cardoso, J. F. (1999). High-Order contrasts for Independent Component Analysis. *Neural Computation*, 11:157–192.

[12] Cardoso, J. F. and Souloumiac, A. (1993). Blind beamforming for non-gaussian signals. *IEE Proceedings*, 140(6):362–370.

[13] Castellazzi, P., Martel, R., Galloway, D. L., Longuevergne, L., and Rivera, A. (2016). Assessing groundwater depletion and dynamics using GRACE and InSAR: potential and limitations. *Groundwater*, 54(6):768–780. doi:10.1111/gwat.12453.

[14] Chen, H., Sun, Y., Gao, J., Hu, Y., and Yin, B. (2018). Solving partial least squares regression via manifold optimization approaches. *IEEE Transactions on Neural Networks and Learning Systems*, pages 1–13. doi:10.1109/TNNLS.2018.2844866.

[15] Chen, J., Famigliett, J. S., Scanlon, B. R., and Rodell, M. (2016). Groundwater storage changes: Present status from GRACE observations. *Surveys in Geophysics*, 37(2):397–417. doi:10.1007/s10712-015-9332-4.

[16] Chen, J. L., Wilson, C. R., Tapley, B. D., Blankenship, D. D., and Ivins, E. R. (2007a). Patagonia Icefield melting observed by Gravity Recovery and Climate Experiment (GRACE). *Geophysical Research Letters*, 34(22):L22501. doi:10.1029/2007GL031871.

[17] Chen, J. L., Wilson, C. R., Tapley, B. D., and Grand, S. (2007b). GRACE detects coseismic and postseismic deformation from the Sumatra-Andaman earthquake. *Geophysical Research Letters*, 34(13):L13302. doi:10.1029/2007GL030356.

[18] Common, P. (1994). Independent component analysis, A new concept? *Signal Processing*, 36:287–314.

[19] Conway, D., Persechino, A., Ardoin-Bardin, S., Hamandawana, H., Dieulin, C., and Mahé, G. (2009). Rainfall and water resources variability in Sub-Saharan Africa during the twentieth century. *Journal of Hydrometeorology*, 10(1):41–59. doi:10.1175/2008JHM1004.1.

[20] de Jong, S. (1993). SIMPLS: An alternative approach to partial least squares regression. *Chemometrics and Intelligent Laboratory Systems*, 18(3):251–263. doi:10.1016/0169-7439(93)85002-x.

[21] de Linage, C., Famiglietti, J. S., and Randerson, J. T. (2014). Statistical prediction of terrestrial water storage changes in the Amazon Basin using tropical Pacific and North Atlantic sea surface temperature anomalies. *Hydrology and Earth System Sciences*, 18(6):2089–2102. doi:10.5194/hess-18-2089-2014.

[22] Dong, L., Shimada, J., Kagabu, M., and Fu, C. (2015). Teleconnection and climatic oscillation in aquifer water level inKumamoto plain, Japan. *Hydrological Processes*, 29(7):1687–1703. doi:10.1002/hyp.10291.

[23] Erfanian, A., Wang, G., and Fomenko, L. (2017). Unprecedented drought over tropical south america in 2016: significantly under-predicted by tropical sst. *Scientific Reports*, 7(5811). doi:10.1038/s41598-017-05373-2.

[24] Famiglietti, J. S. (2014). The global groundwater crisis. *Nature*, 4:945–948. doi:10.1038/nclimate2425.

[25] Famiglietti, J. S., Cazenave, A., Eicker, A., Reager, J. T., Rodell, M., and Velicogna, I. (2015). Satellites provide the big picture. *Science*, 349(6249):684–685. doi:10.1126/science.aac9238.

[26] Famiglietti, J. S. and Rodell, M. (2013). Water in the balance. *Science*, 340(6138):1300–1301. doi:10.1126/science.1236460.

[27] Ferreira, V., Montecino, H., Ndehedehe, C., Heck, B., Gong, Z., Westerhaus, M., and de Freitas, S. (2018). Space-based observations of crustal deflections for drought characterization in brazil. *Science of The Total Environment*, 644:256–273. doi:10.1016/j.scitotenv.2018.06.277.

[28] Ferreira, V. G., Montecino, H. D., Ndehedehe, C. E., del Rio, R. A., Cuevas, A., and de Freitas, S. R. C. (2019). Determining seasonal displacements of Earth's crust in South America using observations from space-borne geodetic sensors and surface-loading models. *Earth, Planets and Space*, 71(1):84. doi:10.1186/s40623-019-1062-2.

[29] Fontaine, B. and Bigot, S. (1993). West African rainfall deficits and sea surface temperatures. *International Journal Of Climatology*, 13(3):271–285. doi:10.1002/joc.3370130304.

[30] Frappart, F., Papa, F., da Silva, J. S., Ramillien, G., Prigent, C., Seyler, F., and Calmant, S. (2012). Surface freshwater storage and dynamics in the Amazon basin during the 2005 exceptional drought. *Environmental Research Letters*, 7(4):044010.

[31] Frappart, F., Papa, F., Guntner, A., Werth, S., da Silva, J. S., Tomasella, J., Seyler, F., Prigent, C., Rossow, W. B., Calmant, S., and Bonnet, M.-P. (2011a). Satellite-based estimates of groundwater storage variations in large drainage basins with extensive floodplains. *Remote Sensing of Environment*, 115(6):1588–1594. doi:10.1016/j.rse.2011.02.003.

[32] Frappart, F., Ramillien, G., Leblanc, M., Tweed, S. O., Bonnet, M.-P., and Maisongrande, P. (2011b). An independent component analysis filtering approach for estimating continental hydrology in the GRACE gravity data. *Remote Sensing of Environment*, 115(1):187 – 204. doi:doi.org/10.1016/j.rse.2010.08.017.

[33] Frappart, F., Ramillien, G., Maisongrande, P., and Bonnet, M.-P. (2010). Denoising satellite gravity signals by independent component analysis. *Geoscience and Remote Sensing Letters, IEEE*, 7(3):421–425. doi:10.1109/LGRS.2009.2037837.

[34] Frappart, F., Ramillien, G., and Ronchail, J. (2013a). Changes in terrestrial water storage versus rainfall and discharges in the amazon basin. *International Journal Of Climatology*, 33:3029—3046. doi:10.1002/joc.3647.

[35] Frappart, F., Seoane, L., and Ramillien, G. (2013b). Validation of GRACE-derived terrestrial water storage from a regional approach over South America. *Remote Sensing of Environment*, 137:69 – 83.

[36] Getirana, A. (2016). Extreme water deficit in brazil detected from space. *Journal of Hydrometeorology*, 17(2):591–599. doi:10.1175/JHM-D-15-0096.1.

[37] Getirana, A., Kumar, S., Girotto, M., and Rodell, M. (2017). Rivers and floodplains as key components of global terrestrial water storage variability. *Geophysical Research Letters*, 44(20):10,359–10,368. doi:10.1002/2017GL074684.

[38] Gutiérrez, A. P. A., Engle, N. L., Nys, E. D., Molejón, C., and Martins, E. S. (2014). Drought preparedness in brazil. *Weather and Climate Extremes*, 3:95 – 106.

[39] Han, S.-C., Kim, H., Yeo, I.-Y., Yeh, P., Oki, T., Seo, K.-W., Alsdorf, D., and Luthcke, S. B. (2009). Dynamics of surface water storage in the Amazon inferred from mea-

surements of inter-satellite distance change. *Geophysical Research Letters*, 36(9):L09403. doi:10.1029/2009GL037910.

[40] Han, S.-C., Sauber, J., and Luthcke, S. (2010). Regional gravity decrease after the 2010 Maule (Chile) earthquake indicates large-scale mass redistribution. *Geophysical Research Letters*, 37(23). doi:10.1029/2010GL045449.

[41] Humphrey, V., Gudmundsson, L., and Seneviratne, S. I. (2016). Assessing global water storage variability from GRACE: trends, seasonal cycle, subseasonal anomalies and extremes. *Surveys in Geophysics*, 37(2):357–395. doi:10.1007/s10712-016-9367-1.

[42] Jaramillo, E., Melnick, D., Baez, J. C., Montecino, H., Lagos, N. A., Acuña, E., Manzano, M., and Camus, P. A. (2017). Calibrating coseismic coastal land-level changes during the 2014 iquique (mw=8.2) earthquake (northern chile) with leveling, gps and intertidal biota. *PLOS One*, 12(3):1–16. doi:10.1371/journal.pone.0174348.

[43] Jarque, C. M. and Bera, A. K. (1980). Efficient tests for normality, homoscedasticity and serial independence of regression residuals. *Economics Letters*, 6(3):255 – 259. doi.org/10.1016/0165-1765(80)90024-5.

[44] Jolliffe, I. T. (2002). Principal component analysis (second edition). *Springer Series in Statistics*. Springer, New York.

[45] Kendall, M. G. (1970). Rank correlation methods. *Griffin, London*, (4th edition). UK.

[46] Kim, H., Yeh, P. J.-F., Oki, T., and Kanae, S. (2009). Role of rivers in the seasonal variations of terrestrial water storage over global basins. *Geophysical Research Letters*, 36(17):L17402. doi:10.1029/2009GL039006.

[47] Krepper, G., Romeo, F., de Sousa Fernandes, D. D., Diniz, P. H. G. D., de Araújo, M. C. U., Nezio, M. S. D., Pistonesi, M. F., and Centurión, M. E. (2018). Determination of fat content in chicken hamburgers using nir spectroscopy and the successive projections algorithm for interval selection in pls regression (ispa-pls). *Spectrochimica Acta Part A: Molecular and Biomolecular Spectroscopy*, 189:300 – 306. note:doi.org/10.1016/j.saa.2017.08.046.

[48] Kroes, J., van Dam, J., Supit, I., de Abelleyra, D., Verón, S., de Wit, A., Boogaard, H., Angelini, M., Damiano, F., Groenendijk, P., Wesseling, J., and Veldhuizen, A. (2019). Agrohydrological analysis of groundwater recharge and land use changes in the Pampas of Argentina. *Agricultural Water Management*, 213:843 – 857. doi:10.1016/j.agwat.2018.12.008.

[49] Lewis-Beck, M., Bryman, A., and Futing, T. (2003). Encyclopedia of social sciences research methods. *Thousand Oaks (CA): Sage*, pages accessed from https://www.utdallas.edu/ herve/Abdi–PLS–pretty.pdf on 4th January 2019.

[50] Linage, C., Kim, H., Famiglietti, J. S., and Yu, J.-Y. (2013). Impact of pacific and atlantic sea surface temperatures on interannual and decadal variations of GRACE land water storage in tropical South America. *Journal of Geophysical Research: Atmospheres*, 118(19):10,811–10,829. doi:10.1002/jgrd.50820.

[51] Lomnitz, C. (2004). Major earthquakes of Chile: A historical survey, 1535-1960. *Seismological Research Letters*, 75(3):368–378. doi:10.1785/gssrl.75.3.368.

[52] Mann, H. B. (1945). Nonparametric tests against trend. *Econometrica*, 13(3):245–259. doi:10.2307/1907187.

[53] Martinez, W. L. and Martinez, A. R. (2005). *Exploratory Data Analysis with MATLAB*. Computer Science and Data Analysis Series. Chapman and Hall/CRC Press LLC, UK.

[54] Montecino, H. D., de Freitas, S. R., Báez, J. C., and Ferreira, V. G. (2017a). Effects on chilean vertical reference frame due to the maule earthquake co-seismic and post-seismic effects. *Journal of Geodynamics*, 112:22 – 30. doi:10.1016/j.jog.2017.07.006.

[55] Montecino, H. D. C., Ferreira, V. G., Cuevas, A., Cabrera, L. C., Báez, J. C. S., and Freitas, S. R. C. D. (2017b). Vertical deformation and sea level changes in the coast of chile by satellite altimetry and tide gauges. *International Journal of Remote Sensing*, 38(24):7551–7565. doi:10.1080/01431161.2017.1288306.

[56] Moore, P. and Williams, S. D. P. (2014). Integration of altimetry lake lavels and GRACE gravimetry over Africa: Inferences for terrestrial water storage change 2003-2011. *Water Resources Research*, 50:9696–9720. doi:10.1002/2014WR015506.

[57] Nash, J. and Sutcliffe, J. (1970). River flow forecasting through conceptual models part i: A discussion of principles. *Journal of Hydrology*, 10(3):282 – 290. doi:10.1016/0022-1694(70)90255-6.

[58] Ndehedehe, C., Awange, J., Agutu, N., Kuhn, M., and Heck, B. (2016a). Understanding changes in terrestrial water storage over West Africa between 2002 and 2014. *Advances in Water Resources*, 88:211–230. doi:10.1016/j.advwatres.2015.12.009.

[59] Ndehedehe, C. E. (2019). The water resources of tropical West Africa: propblems, progress and prospect. *Acta Geophysica*, 67(2):621–649. https://doi.org/10.1007/s11600-019-00260-y.

[60] Ndehedehe, C. E., Agutu, N. O., Okwuashi, O. H., and Ferreira, V. G. (2016b). Spatio-temporal variability of droughts and terrestrial water storage over Lake Chad Basin using independent component analysis. *Journal of Hydrology*, 540:106–128. doi:10.1016/j.jhydrol.2016.05.068.

[61] Ndehedehe, C. E., Anyah, R. O., Alsdorf, D., Agutu, N. O., and Ferreira, V. G. (2019). Modelling the impacts of global multi-scale climatic drivers on hydro-climatic extremes (1901–2014) over the Congo basin. *Science of The Total Environment*, 651:1569 – 1587. doi:10.1016/j.scitotenv.2018.09.203.

[62] Ndehedehe, C. E., Awange, J., Kuhn, M., Agutu, N., and Fukuda, Y. (2017a). Analysis of hydrological variability over the Volta river basin using in-situ data and satellite observations. *Journal of Hydrology: Regional studies*, 12:88–110. doi:10.1016/j.ejrh.2017.04.005.

[63] Ndehedehe, C. E., Awange, J., Kuhn, M., Agutu, N., and Fukuda, Y. (2017b). Climate teleconnections influence on West Africa's terrestrial water storage. *Hydrological Processes*, 31(18):3206–3224. doi: 10.1002/hyp.11237.

[64] Ndehedehe, C. E., Awange, J. L., Agutu, N. O., and Okwuashi, O. (2018). Changes in hydro-meteorological conditions over tropical West Africa (1980 – 2015) and links to global climate. *Global and Planetary Change*, 162:321–341. doi:10.1016/j.gloplacha.2018.01.020.

[65] Ni, S., Chen, J., Wilson, C. R., Li, J., Hu, X., and Fu, R. (2018). Global terrestrial water storage changes and connections to ENSO events. *Surveys in Geophysics*, 39(1):1–22. doi:10.1007/s10712-017-9421-7.

[66] Nicholson, S. (2013). The West African Sahel: a review of recent studies on the rainfall regime and its interannual variability. *ISRN Meteorology*, 2013(453521):1–32. doi:10.1155/2013/453521.

[67] Nka, B. N., Oudin, L., Karambiri, H., Paturel, J. E., and Ribstein, P. (2015). Trends in floods in West Africa: analysis based on 11 catchments in the region. *Hydrology and Earth System Sciences*, 19(11):4707–4719. doi:10.5194/hess-19-4707-2015.

[68] Odekunle, T. O. and Eludoyin, A. O. (2008). Sea surface temperature patterns in the Gulf of Guinea: their implications for the spatio-temporal variability of precipitation in West Africa. *International Journal Of Climatology*, 28:1507–1517. doi:10.1002/joc.1656.

[69] Paeth, H., Fink, A., Pohle, S., Keis, F., Machel, H., and Samimi, C. (2012). Meteorological characteristics and potential causes of the 2007 flood in sub-Saharan Africa. *International Journal of Climatology*, 31:1908–1926. doi:10.1002/Joc.2199.

[70] Phillips, T., Nerem, R. S., Fox-Kemper, B., Famiglietti, J. S., and Rajagopalan, B. (2012). The influence of ENSO on global terrestrial water storage using GRACE. *Geophysical Research Letters*, 39:L16705. doi:10.1029/2012GL052495, 2012.

[71] Preisendorfer, R. (1988). Principal component analysis in meteorology and oceanography. *Developments in Atmospheric Science 17*. Elsevier, Amsterdam.

[72] Ramillien, G. L., Seoane, L., Frappart, F., Biancale, R., Gratton, S., Vasseur, X., and Bourgogne, S. (2012). Constrained regional recovery of continental water mass time-variations from GRACE-based geopotential anomalies over South America. *Surveys in Geophysics*, 33(5):887–905. doi:10.1007/s10712-012-9177-z.

[73] Reager, J. T., Thomas, B. F., and Famiglietti, J. S. (2014). River basin flood potential inferred using GRACE gravity observations at several months lead time. *Nature Geoscience*, 7(8):588–592. doi:10.1038/ngeo2203.

[74] Rieser, D., Kuhn, M., Pail, R., Anjasmara, I. M., and Awange, J. (2010). Relation between GRACE-derived surface mass variations and precipitation over Australia. *Australian Journal of Earth Sciences*, 57(7):887–900. doi:10.1080/08120099.2010.512645.

[75] Rodell, M., Famiglietti, J. S., Wiese, D. N., Reager, J. T., Beaudoing, H. K., Landerer, F. W., and Lo, M.-H. (2018). Emerging trends in global freshwater availability. *Nature*, 557:651–659. doi:10.1038/s41586-018-0123-1.

[76] Ruiz, S. and Madariaga, R. (2018). Historical and recent large megathrust earthquakes in Chile. *Tectonophysics*, 733:37 – 56. doi:10.1016/j.tecto.2018.01.015.

[77] Save, H., Bettadpur, S., and Tapley, B. D. (2016). High-resolution CSR GRACE RL05 mascons. *Journal of Geophysical Research: Solid Earth*, 121(10):7547–7569. doi:10.1002/2016JB013007.

[78] Schneider, U., Becker, A., Finger, P., Meyer-Christoffer, A., Ziese, M., and Rudolf, B. (2014). GPCC's new land surface precipitation climatology based on quality-controlled in situ data and its role in quantifying the global water cycle. *Theoretical and Applied Climatology*, 115(1-2):15–40. doi:10.1007/s00704-013-0860-x.

[79] Semazzi, F. H. M., Mehta, V., and Sud, Y. (1988). An investigation of the relationship between sub-Saharan rainfall and global sea surface temperatures. *Atmosphere-Ocean*, 26(1):118–138. doi:10.1080/07055900.1988.9649293.

[80] Sen, P. K. (1968). Estimates of the regression coefficient based on Kendall's Tau. *Journal of the American Statistical Association*, 63(324):1379–1389. doi:10.1080/01621459.1968.10480934.

[81] Sheffield, J. and Wood, E. F. (2008). Global trends and variability in soil moisture and drought characteristics, 1950–2000, from observation-driven simulations of the terrestrial hydrologic cycle. *Journal of Climate*, 21(3):432–458. doi:10.1175/2007JCLI1822.1.

[82] Snedecor, G. W. and Cochran, W. G. (1989). Statistical methods. *Iowa State University Press*, 8th Edition.

[83] Spinoni, J., Naumann, G., Carrao, H., Barbosa, P., and Vogt, J. (2014). World drought frequency, duration, and severity for 1951–2010. *International Journal of Climatology*, 34(8):2792–2804. doi:10.1002/joc.3875.

[84] Sun, T., Ferreira, V. G., He, X., and Andam-Akorful, S. A. (2016). Water availability of São Francisco river basin based on a space-borne geodetic sensor. *Water*, 8(5).

[85] Swenson, S. and Wahr, J. (2002). Methods for inferring regional surface-mass anomalies from Gravity Recovery and Climate Experiment (GRACE) measurements of time-variable gravity. *Journal of Geophysical Research-Solid Earth*, 107(B9). doi:10.1029/2001jb000576.

[86] Swenson, S. and Wahr, J. (2007). Multi-sensor analysis of water storage variations of the Caspian Sea. *Geophysical Research Letters*, 34(16). doi:10.1029/2007gl030733.

[87] Tapley, B., Bettadpur, S., Watkins, M., and Reigber, C. (2004). The Gravity Recovery and Climate Experiment: Mission overview and early results. *Geophysical Research Letters*, 31:1–4. doi:10.1029/ 2004GL019920.

[88] Thomas, A. C., Reager, J. T., Famiglietti, J. S., and Rodell, M. (2014). A GRACE-based water storage deficit approach for hydrological drought characterization. *Geophysical Research Letters*, 41(5):1537–1545. 10.1002/2014GL059323.

[89] Tourian, M. J., Reager, J. T., and Sneeuw, N. (2018). The total drainable water storage of the Amazon River Basin: A first estimate using GRACE. *Water Resources Research*, 54(5):3290–3312. doi:10.1029/2017WR021674.

[90] van der Molen, M., Dolman, A., Ciais, P., Eglin, T., Gobron, N., Law, B., Meir, P., Peters, W., Phillips, O., Reichstein, M., Chen, T., Dekker, S., Doubková, M., Friedl, M., Jung, M., van den Hurk, B., de Jeu, R., Kruijt, B., Ohta, T., Rebel, K., Plummer, S., Seneviratne, S., Sitch, S., Teuling, A., van der Werf, G., and Wang, G. (2011). Drought and ecosystem carbon cycling. *Agricultural and Forest Meteorology*, 151(7):765 – 773. doi:10.1016/j.agrformet.2011.01.018.

[91] Vigny, C., Socquet, A., Peyrat, S., Ruegg, J.-C., Métois, M., Madariaga, R., Morvan, S., Lancieri, M., Lacassin, R., Campos, J., Carrizo, D., Bejar-Pizarro, M., Barrientos, S., Armijo, R., Aranda, C., Valderas-Bermejo, M.-C., Ortega, I., Bondoux, F., Baize, S., Lyon-Caen, H., Pavez, A., Vilotte, J. P., Bevis, M., Brooks, B., Smalley, R., Parra, H., Baez, J.-C., Blanco, M., Cimbaro, S., and Kendrick, E. (2011). The 2010 mw 8.8 Maule megathrust earthquake of Central Chile, monitored by GPS. *Science*, 332(6036):1417–1421. doi:10.1126/science.1204132.

[92] Vorosmarty, C. J., McIntyre, P. B., Gessner, M. O., Dudgeon, D., Prusevich, A., Green, P., Glidden, S., Bunn, S. E., Sullivan, C. A., Liermann, C. R., and Davies, P. M. (2010). Global threats to human water security and river biodiversity. *Nature*, 467:555–555–561. doi:10.1038/nature09440.

[93] Wada, Y., Bierkens, M. F. P., de Roo, A., Dirmeyer, P. A., Famiglietti, J. S., Hanasaki, N., Konar, M., Liu, J., Müller Schmied, H., Oki, T., Pokhrel, Y., Sivapalan, M., Troy, T. J., van Dijk, A. I. J. M., van Emmerik, T., Van Huijgevoort, M. H. J., Van Lanen, H. A. J., Vörösmarty, C. J., Wanders, N., and Wheater, H. (2017). Human-water interface in hydrological modelling: current status and future directions. *Hydrology and Earth System Sciences*, 21(8):4169–4193. doi:10.5194/hess-21-4169-2017.

[94] Wahr, J., Molenaar, M., and Bryan, F. (1998). Time variability of the Earth's gravity

field: Hydrological and oceanic effects and their possible detection using GRACE. *Journal of Geophysical Research-Solid Earth*, 103(B12):30205–30229. doi:10.1029/98jb02844.

[95] Watkins, M. M., Wiese, D. N., Yuan, D., Boening, C., and Landerer, F. W. (2015). Improved methods for observing earth's time variable mass distribution with GRACE using spherical cap mascons. *Journal of Geophysical Research: Solid Earth*, 120(4):2648–2671. doi:10.1002/2014JB011547.

[96] Wiese, D. N., Landerer, F. W., and Watkins, M. M. (2016). Quantifying and reducing leakage errors in the JPL RL05M GRACE mascon solution. *Water Resources Research*, 52(9):7490–7502.

[97] Willis, M. J., Melkonian, A. K., Pritchard, M. E., and Ramage, J. M. (2012). Ice loss rates at the Northern Patagonian icefield derived using a decade of satellite remote sensing. *Remote Sensing of Environment*, 117:184 – 198. doi:10.1016/j.rse.2011.09.017.

[98] Willmott, C. J., Robeson, S. M., and Matsuura, K. (2012). A refined index of model performance. *International Journal of Climatology*, 32(13):2088–2094. doi:10.1002/joc.2419.

[99] Wold, S., Sjöström, M., and Eriksson, L. (2001). PLS-regression: a basic tool of chemometrics. *Chemometrics and Intelligent Laboratory Systems*, 58(2):109 – 130. doi:10.1016/S0169-7439(01)00155-1.

[100] Wouters, B., Bonin, J. A., Chambers, D. P., Riva, R. E. M., Sasgen, I., and Wahr, J. (2014). GRACE, time-varying gravity, Earth system dynamics and climate change. *Reports on Progress in Physics*, 77(11):116801. doi:10.1088/0034-4885/77/11/116801.

[101] Zarfl, C., Lumsdon, A. E., Berlekamp, J., Tydecks, L., and Tockner, K. (2015). A global boom in hydropower dam construction. *Aquatic Sciences*, 77:161–170. doi:10.1007/s00027-014-0377-0.

[102] Ziehe, A. (2005). Blind source separation based on joint diagonalization of matrices with applications in biomedical signal processing. *PhD thesis,Universitat Potsdam.* Retrieved from:http://en.youscribe.com/catalogue/reports-and-theses/knowledge/blind-source-separation-based-on-joint-diagonalization-of-matrices-1424347. Accessed 15 May 2015.

[103] Zou, Y., Macau, E. E. N., Sampaio, G., Ramos, A. M. T., and Kurths, J. (2018). Characterizing the exceptional 2014 drought event in são paulo by drought period length. *Climate Dynamics*, 51(1):433–442. doi:10.1007/s00382-017-3932-2.